This manuscript is a preprint and has been submitted for publication in Basin Research. This manuscript has not yet been through peer review. Subsequent versions of this manuscript may have slightly different content. If accepted, the final version of this manuscript will be available via the 'Peer-reviewed Publication DOI' link on the right-hand side of this webpage. Please feel free to contact any of the authors; we welcome feedback.

Obstructed Minibasins on a Salt-Detached Slope: An Example from above the Sigsbee Canopy, Northern Gulf of Mexico

Oliver B. Duffy[a*], Naiara Fernandez[a], Frank J. Peel[a], Michael R. Hudec[a], Tim P. Dooley[a], Christopher A-L Jackson[b]

[a]*Bureau of Economic Geology, Jackson School of Geosciences, The University of Texas at Austin, University Station, Box X, Austin, Texas, 78713-8924, USA*
[b]*Basins Research Group (BRG), Department of Earth Science & Engineering, Imperial College, Prince Consort Road, London, United Kingdom, SW7 2BP, UK*

** Corresponding Author: oliver.duffy@beg.utexas.edu*

Keywords: salt tectonics; welding; supra-salt strain; base-of-salt relief; shortening; extension; salt-detached slopes

Highlights

- The salt-detached slope above the Sigsbee Canopy in the northern Gulf of Mexico is influenced by a rugose base-of-salt
- We examine how downslope-translating supra-canopy minibasins interact with the rugose base-of-salt
- Basal minibasin welds obstruct the downslope translation of minibasins and control supra-salt strain patterns
- Typically, an obstructed minibasin shows shortening to its immediate upslope and extension to its downslope

- Minibasins can be obstructed to different degrees, likely resulting in differential minibasin translation

Abstract

Salt-detached gravity-gliding/spreading systems having a rugose base-of-salt display complex strain patterns. However, little was previously known about how welding of supra-salt minibasins to the sub-salt may influence both the downslope translation of minibasins on salt-detached slopes and the regional pattern of supra-salt strain. Using a regional 3D seismic reflection data set, we examine a large salt-stock canopy system with a rugose base on the northern Gulf of Mexico slope, on which minibasins both subside and translate downslope. Some minibasins are welded at their bases, and others are not. We suggest that basal welds obstruct downslope translation of minibasins and control regional patterns of supra-canopy strain.

The distribution of strain above the canopy is complex and variable. Each minibasin that becomes obstructed modifies the local strain field, typically developing a zone of shortening immediately updip and an extensional breakaway zone immediately downdip. This finding is corroborated by observations from a physical sandbox model of minibasin obstruction. We also find in our natural example that minibasins can be obstructed to different degrees, ranging from severe (e.g. caught in a feeder) to mild (e.g. welded to a flat or gently-dipping base-of-salt). By mapping both the presence of obstructed minibasins, and the relative degree of minibasin obstruction, we provide an explanation for the origin of complex 3-D strain fields on a salt-detached slope and, potentially, a mechanism that explains differential downslope translation of

minibasins. In minibasin-rich salt-detached slope settings, our results may aid: i) structural restorations and regional strain analyses; ii) prediction of subsalt relief in areas of poor seismic imaging; and iii) prediction of stress fields and borehole stability. Our findings are applicable to other systems detached on allochthonous salt sheets (e.g. Gulf of Mexico; Scotian Margin, offshore eastern Canada), as well as systems where the salt is autochthonous but has significant local basal relief (e.g. Santos Basin, offshore Brazil; Kwanza Basin, Angola).

1. Introduction

Salt-detached gravity-gliding/spreading systems with a relatively smooth base-of-salt have commonly been interpreted in terms of kinematically-linked domains of upslope extension and downslope shortening, which may be connected by a domain of midslope translation (Fig. 1a) (e.g. Cobbold and Szatmari, 1991; Brun and Fort 2004, 2011; Hudec and Jackson, 2004; Rowan et al., 2004; Peel, 2014; Jackson et al. 2015). However, recent work has shown that strain patterns are more complex where translation occurs above base-of-salt relief; this occurs for two reasons. First, if a base-of-salt high fully protrudes above the salt at the onset of gliding, it may block downslope flow of salt and its overburden. This may partition the salt-detached slope system into extensional-contractional sub-systems (Fig. 1b) (e.g. Loncke et al., 2006; Ferrer et al., 2017). Second, localized zones of contraction and extension can occur anywhere on a slope where salt and an overburden are gliding downslope above base-of-salt relief (Fig. 1b) (e.g. Cobbold and Szatmari, 1991; Gaullier et al., 1993; Dooley et al 2017; 2018; Dooley and Hudec, 2017). As salt crosses the base-of-salt relief, local acceleration and deceleration of the salt due to flux mismatches generates zones

of contraction and extension of the overburden (Dooley et al 2017; 2018; Dooley and Hudec, 2017).

The models above assume the overburden is largely detached from subsalt strata during downslope transport. However, a factor complicating the downslope translation of salt-detached slopes is minibasin welding (Krueger, 2010). In this study we use a 3D seismic reflection data set to examine a salt-stock canopy system on the northern Gulf of Mexico slope. A population of minibasins have subsided or are actively subsiding into, and have translated downslope above, an extremely rugose base-of-salt. This structural setting differs from the salt-detached slopes described in prior related studies in three key ways (e.g. Gaullier et al., 1993, Loncke et al., 2006, Dooley et al., 2017, Dooley and Hudec, 2017, and Ferrer et al., 2017). First, rather than having a prekinematic supra-canopy interval of fairly uniform thickness, the supra-canopy is instead composed of minibasins of variable thickness. Second, there is base-of-salt surface shows relief of >10 km in places due to the presence of feeders that connect down to the deep (autochthonous) salt. Third, rather than just one irregularity in the base-of-salt (e.g. the Eratosthenes Seamount in Loncke et al., 2006), the study area contains a large number of structural highs and lows that vary in height, spacing and flank gradient. Such a scenario leads to the possibility that if thick enough, supra-canopy minibasins will interact with the many highs and lows on the base-of-salt surface, as well as with one another. In particular, base-of-salt highs may obstruct the minibasins from translating freely downslope. Our study area thus provides an ideal setting to address the structural styles of obstructed minibasins, and how they affect the pattern of supra-canopy strain in salt-detached slopes. Our findings are applicable to a number of salt-detached slopes where minibasins and extreme base-of-salt relief occur (e.g. Gulf of Mexico, the Scotian Margin (offshore eastern Canada), offshore of the South Atlantic Margins, offshore Morocco).

2. Geological Context

2.1. Evolution of the Gulf of Mexico

The Gulf of Mexico basin began forming in the Late Triassic due to NW-SE-oriented rifting as South America split from North America during the breakup of Pangea (e.g. Pindell and Dewey, 1982; Marton and Buffler, 1994). Subsequent Late Jurassic and Early Cretaceous rifting saw the formation of new oceanic crust as the Yucatan Block moved away from North America and rotated counterclockwise (e.g. Pindell, 1985; Buffler, 1991; Pindell and Kennan, 2009; Pindell et al 2014; Rowan, 2014). Isolation from greater oceanic circulation during rifting drove deposition of the Louann Salt (e.g. Salvador, 1991; Konyukhov, 2008; Bouroullec and Weimer, 2017; Curry et al., 2018). The Louann Salt shows significant variability in its distribution and thickness due to the rift-related seafloor topography on which it was deposited (Wu et al., 1990; Tew et al., 1991; Salvador, 1991; Peel et al., 1995; Mondelli, 2010; Hudec et al., 2013). Following an increased influx of ocean water into the Gulf that prohibited further salt deposition (Carter et al., 2016), Mesozoic deposition in the Gulf of Mexico was dominated by marine carbonates, with pulses of localized clastic input (Winker and Buffler, 1988; Galloway, 2008; Galloway et al, 2011). During the Cenozoic, large volumes of clastics were deposited that: i) loaded the basement such that it subsided deeply; and ii) forced the shelf margin to prograde several hundred kilometers (e.g., Peel et al., 1995; Galloway et al., 2000; Galloway, 2008).

2.2. Salt-Tectonic Context of the northern Gulf of Mexico

This study focuses on the mid-to-lower slope of part of the northern Gulf of Mexico (Fig. 2). The precise location of the study area cannot be revealed for data-confidentiality reasons, leading us to

present all maps and sections with false geographic orientations (see below). In the study area, gliding- and spreading-induced deformation of Louann Salt began in the Late Jurassic (e.g. Jackson and Talbot, 1991; Diegel et al., 1995; Peel et al, 1995; Rowan et al., 2004; Hudec et al 2013; Bouroullec et al., 2017). Salt diapirs formed between early-formed minibasins and fed a large allochthonous salt body (the Sigsbee salt canopy; e.g. Diegel et al., 1995; Peel et al., 1995; Rowan, 1995; Pilcher et al., 2011; Bouroullec and Weimer, 2017). Neogene to recent sediments subsequently loaded the Sigsbee canopy forming supra-canopy minibasins, the configuration of which are expressed on the pockmarked seafloor (Figs. 2 and 3) (e.g. Peel et al., 1995; Pilcher et al., 2011). Critically, as well as subsiding, the supra-canopy minibasins are also translating downslope gravitationally, a process facilitated by downslope flowage of salt (e.g., Peel et al., 1995; Mount et al., 2007; Krueger, 2010; Hudec et al., 2013).

3. Dataset and Methods

We focus on an area of 13,101 km^2 that is covered by two 3D prestack, depth-migrated, seismic reflection surveys that image to 18 km (Fig. 3). The seismic data provided by WesternGeco Multiclient and CGG are commercially sensitive, so the precise geographic location cannot be released. All maps are rotated, with “north” arbitrarily defined as up on the maps for ease of description. Despite these restrictions, we can say that the study area lies in a mid-to-lower slope setting in the northern Gulf of Mexico. The seismic data are presented such that a downward increase in acoustic impedance is marked by a peak (black on seismic sections) and a downward decrease in acoustic impedance is marked by a trough (white on seismic sections). We mapped the top and base of the Sigsbee canopy across the study area (Fig. 3).

4. Salt-Tectonic Structure

In most places, the base Sigsbee Canopy corresponds to the top of the primary minibasins (Figs. 3 and 4a). However, where feeders are present, the base Sigsbee canopy extends downwards to connect to the top of the deep salt or its equivalent weld (Figs. 3 and 4a). As such, the mapped surface is diachronous and highly rugose, displaying over 15 km of relief, and with dips ranging from 0° to >90° (i.e. diapirs feeding the canopy have upward-flaring, overhanging heads (Fig. 4a; *sensu* Fig 3). In map-view, feeders are sub-circular to elliptical, with the former typically being 5-12 km in diameter, although the long axes of some of the more elliptical feeders may be up to 30 km (Fig. 4a). In general, the base Sigsbee canopy surface expresses an egg-crate-like morphology (Fig. 4a).

5. Distribution of Supra-Canopy Extension and Shortening

To understand how supra-canopy minibasins translate across a rugose base-of-salt detachment and how this influences patterns of overburden strain, we first delineated areas of extension and shortening in the supra-canopy. Areas containing landward or seaward-dipping, predominantly dip-slip normal faults formed in zones of bulk extension (Figs. 5a and b). These faults typically detach downwards into the top of the Sigsbee salt canopy. In contrast, areas with folds, thrusts, squeezed diapirs (e.g. narrow diapirs with arched roofs and teardrop shapes) and sub-vertical secondary welds likely formed in zones of bulk shortening (Figs. 5c-f) (e.g. Brun and Fort 2004; Roca et al., 2006; Dooley et al., 2009; Duffy et al., 2017; 2018; Granado et al., 2018). Note that

183 areas where small outer-arc extensional faults form in zones of bulk shortening are classified as
184 zones of shortening.

185 We note that the zones of supra-canopy extension and shortening described above are *not*
186 spatially partitioned as we might expect based on a classic three-division structural model of salt-
187 detached gravity-gliding/spreading systems. Given that the setting is in the mid-to-lower slope, we
188 may expect a predominance of translation and shortening. However, although shortening is
189 expressed at the toe of the system near the Sigsbee frontal escarpment, the distribution of strain
190 further updip is patchy and complex (Fig. 6). What is controlling this complex map-view
191 distribution of extension and shortening?

192

193

194 # 6. Role of Obstructed Minibasins in Controlling the Distribution of Supra-
195 Canopy Strain

196

197 ### *6.1. How can Minibasin Welding Modify Supra-Canopy Strain Patterns?*

198 If we look at the map of supra-canopy strain we see that shortening zones commonly occur
199 updip of supra-canopy minibasins (structural lows on the top Sigsbee Canopy surface) and
200 extensional zones commonly occur downdip of minibasins (e.g. A-E on Fig 6). Why is this? We
201 propose here, in support of an initial concept presented by Krueger (2010), that when minibasins
202 weld to the base-of-salt, two processes may obstruct minibasins from freely translating downslope:
203 i) the increased frictional resistance at their bases; and/or ii) the buttressing that occurs when
204 minibasins collide with steeply-dipping base-of-salt features (Fig. 7). Thus, salt and any unwelded

minibasins from further upslope will typically continue translating downslope under gravity. These run into the upslope flanks of welded minibasins, which thereby become zones of shortening (Fig. 7). In contrast, downslope of welded minibasins, salt and unwelded minibasins may continue to move downslope, forming extensional breakaways on the downslope flanks of welded minibasins (Fig. 7).

This concept is corroborated by a simple physical model of minibasins on a salt-detached slope (Figs. 8 and 9; see appendix 1 for details on model). In the model, Minibasin 1 becomes obstructed due to welding against a base-of-salt ramp having previously freely translated downslope above relatively thick salt (Figs. 8 and 9). Minibasin 2, located upslope and also originally translating freely downslope above thick salt, runs into the back of the obstructed minibasin, forming an intervening thrust belt (Figs. 8 and 9). In addition, material downslope of Minibasin 1 is able to continue to move freely downslope of the obstructed minibasin, with the zone between the two being characterised by extensional strains (Figs. 8 and 9). On this basis, we classify any minibasin that has its base welded to the base-of-salt as 'obstructed' and typically, though not always, these will show zones of shortening and extension to their immediate upslope and downslope, respectively. In contrast, minibasins that are not welded to the base-of-salt or other obstructed minibasins further downdip, are not restricted from translating downslope. These are termed 'unobstructed' minibasins.

6.2. Style and Distribution of Obstructed Minibasins

If we now look at seismic cross-sections oriented parallel to the inferred downslope translation (line locations are withheld for data confidentiality reasons) we see a variety of styles of obstructed minibasins in our study area (Fig. 10). We find examples where: i) a minibasin has

subsided into a major feeder to become a bucket minibasin that is welded on its flanks to, and obstructed by, an 8.5 km high sub-vertical feeder wall (Fig. 10a); ii) minibasins are welded to, and obstructed by, moderately-to-steeply-landward-dipping highs on the base-of-salt (15-55° dip and 1.2-3.75 km high in the examples shown in Figs. 10b and c); and iii) a minibasin is welded at its base to, and obstructed by, a gently landward-dipping (<10°) top of the primary minibasin (e.g. Fig. 10d). In all three examples, the downslope sides of the obstructed minibasins are defined by zones of extensional breakaway (Figs 10a-d). In contrast, the modes of upslope shortening are more variable. In some cases upslope shortening is expressed by sub-vertical welds between upslope minibasins and the obstructed minibasins; this indicates the two minibasins were previously separated by salt diapirs (Figs. 10a and b). In other cases, shortening is expressed by the upslope minibasins or supra-canopy stratigraphy overthrusting the downslope obstructed minibasins (Figs. 10c-d).

Systematic examination of slope-parallel cross-sections, reveals that obstructed minibasins are common and relatively evenly distributed across the study area (Fig. 11). If we overlay the map of supra-canopy extension and shortening onto the map of the obstructed minibasins (Fig. 12) it is striking that the vast majority of the latter show zones of shortening on their upslope sides and extension on their downslope sides (Fig. 12). The clearest examples of this strain pattern around obstructed minibasins are shown at locations 1-9 in Figure 12. We therefore conclude that the presence and ubiquity of obstructed minibasins across the study area explains most of the complex distribution of extensional and shortening strains (Fig. 12).

There is undoubtedly a strong correlation between the location of obstructed minibasins and the patterns of supra-canopy extensional and shortening strain. However, should we expect that *every* obstructed minibasin will be associated with upslope shortening and downslope

extension? The simple answer to this is ‘no’ as we can separate those obstructed minibasins that adhere to the expected strain pattern (red minibasins in Fig. 13) from those that do not (blue minibasins in Fig. 13). This raises the question: why do some, albeit few (only 3 examples are noted), obstructed minibasins not influence supra-canopy strain in the manner expected? We now briefly explore some of the main potential causes.

First, the high degree of shortening at the edge of the Sigsbee Canopy may propagate upslope from the frontal escarpment and overwhelm the local effects of the relatively local strain field produced by minibasin obstruction. This may explain why the obstructed minibasin located near the Sigsbee escarpment in the ‘east’ does not display a well-developed extensional breakaway on its downslope side (Fig. 13). Second, if a minibasin becomes obstructed at a time when there is no roof on the surrounding diapirs, then any updip shortening and downslope extension may be difficult to detect as it will be accommodated solely by cryptic deformation within the salt (*sensu* Jackson et al., 2015). Third, if an obstructed minibasin is surrounded by numerous other closely-spaced obstructed minibasins, especially those that are severely obstructed, a shadowing effect may occur whereby the local canopy salt is relatively immobile and the supra-canopy roof is pinned in place. As such, the expected upslope shortening zones and downslope extensional breakaways may not develop (e.g. obstructed minibasin W in Figure 13).

6.3. Variations in the Degree of Minibasin Obstruction

We have demonstrated that obstructed minibasins are ubiquitous across the study area and that they can explain complex supra-canopy strains. So far, however, we have not considered the striking differences in the degree to which minibasins are obstructed and the potential implications this may have upon the structural evolution of a salt-detached gravity-gliding/spreading slope.

Using slope-parallel seismic cross-sections, we now describe differences in the degree to which minibasins are obstructed. We classify the degree to which minibasins are obstructed as either *severe*, *high*, *moderate* or *mild* (Fig. 10). We describe severely-obstructed minibasins before progressing to more mildly-obstructed examples.

We classify a supra-canopy minibasin as *severely obstructed* where the downslope flank of the minibasin is welded, and buttressed, against a sub-vertical structural high on the base-of-salt (8.5 km high) (Fig. 10a). A minibasin becomes severely obstructed if it subsides deep into a feeder to form either a bucket or bowl minibasin. In the example shown in Fig. 10a, the downslope translation of the supra-salt minibasin is obstructed by the 8.5 km high sub-vertical feeder wall. We classify a supra-canopy minibasin as *highly obstructed* where a minibasin is welded, and buttressed, against a steeply landward-dipping structural high on the base-of-salt (~55° dip and at least 3.75 km high in the example shown in Figure 10b). If a minibasin is obstructed from translating downslope by being welded to a moderately landward-dipping high on the base-of-salt (~15° dip and at least 1.2 km high in the example shown in Figure 10c) then the minibasin is classified as *moderately obstructed*. Finally, a *mildly-obstructed* minibasin refers to one welded at its base to a flat, or gently landward- or seaward-dipping (e.g. 0-10°) ramp in the base-of-salt (e.g. Figs. 9 and 10d). A map showing the distribution of obstructed minibasins, with the minibasins color-coded according to the degree to which they are obstructed is shown in Figure 14. This map shows significant local variations in the degree of obstruction between adjacent minibasins. For example, minibasins X, Y and Z are trapped in feeders and thus severely-obstructed, yet immediately adjacent to each of these are mildly-obstructed minibasins (Fig. 14).

Intuitively, different degrees of minibasin obstruction should lead to differences in minibasin mobility. The physical-modeling results shown in Figures 8 and 9 suggest that mildly-

297 to moderately-obstructed minibasins can, under some circumstances, continue translating
298 downslope after welding. For example, after 42 hours of the model run (Fig. 8c), Minibasin 1 was
299 obstructed from moving downslope by the base-of-salt ramp. A major fold-and-thrust belt
300 developed on its upslope side as the more mobile Minibasin 2 converged (Fig. 8c). However, after
301 260 hours, despite having welded to the ramp, Minibasin 1 translated further downslope, coming
302 to rest on earlier-deposited roof material (Fig. 9). We envisage two ways in which an obstructed
303 minibasin may partially or fully overcome moderate-to-mild base-of-salt obstructions: i) the
304 gravitational 'push' from the downslope-translating salt and supra-salt units located on its upslope
305 side, an effect that would increase if the dip of the margin increased; ii) salt inflation at the
306 downslope portion of the slope, a process that may passively uplift or remobilize the otherwise
307 obstructed minibasin. Overall, moderately-to-mildly obstructed minibasins have a much greater
308 potential to translate downslope after obstruction, than severely- or highly-obstructed minibasins.
309 The likely differential translation of minibasins obstructed to different degrees should be
310 accommodated by 3D strains and deformation. Kruger (2010) suggests that lateral tear faults
311 (*sensu* Rowan et al., 1999) could form at the boundaries between minibasins that have different
312 mobilities. A more detailed examination of the evidence for differential translation in supra-canopy
313 minibasin systems forms the basis of a companion paper (Fernandez et al., *in prep*).
314

315 ## 7. Supra-Salt Strain Patterns and Kinematics in Salt-Detached Slope Settings

316

317 In the early stages of margin development when minibasins are relatively thin and do not interact
318 with the base-of-salt relief, the structural zonation of the salt-detached slope is expected to be

relatively simple (Fig. 15a). In contrast, later in margin development, when minibasins are thick enough such that their bases weld to the base-of-salt, they become obstructed. During the latter stage a more complex strain pattern develops, with shortening strains typically developed immediately upslope of each obstructed minibasin and an extensional breakaway developed immediately downslope (Fig. 15b). Furthermore, minibasins can be obstructed to different degrees (Fig. 15b). Thus, we propose that minibasin obstruction exerts a first-order control on the mobility of minibasins and the pattern of supra-canopy strain.

We now compare the structural styles, processes and strain patterns observed on in the supra-canopy of the Northern Gulf of Mexico slope to previous studies of salt-detached slope systems. First, in this study, many supra-canopy minibasins are subsiding and translating downslope above a base-of-salt with many closely-spaced, three-dimensionally complex, structural highs and lows. This results in a high incidence of basal welds and sub-vertical welds on the minibasin margins that prevent minibasins from translating further downslope and locally modify the strain field. The slope is thus partitioned into many extensional-contractional gravitational sub-systems (or 'flow cells') developed between the obstructions, many of which only extend for 10-15 km along-strike. This contrasts markedly with examples from the Liguro-Provencal Basin (Ferrer et al., 2017) and the Nile Deep Sea Fan (Loncke et al., 2006), in which the base-of-salt has only a few major obstructions (in these cases, volcanic seamounts). These slope systems are partitioned into fewer and much larger-scale extensional-contractional gravitational sub-systems. For example, in the case of the Nile Deep Sea Fan system, the Eratosthenes Seamount modifies the supra-salt strain pattern over thousands of square kilometres (e.g. Loncke et al. 2006; Allen et al., 2016).

Second, in this study, the base-of-salt relief is both positive and negative relative to the regional flat-lying tops of the primary minibasins, with the negative relief marked by feeders (Figs. 3 and 4a). It is striking how severely-obstructed minibasins are trapped and enclosed within the negative relief of the feeders (Fig. 10a). It is highly unlikely these severely-obstructed minibasins will ever move. In contrast, when the obstruction is defined by positive relief, such as an isolated base-of-salt high (this study) or a volcanic seamount (Loncke et al., 2006; Ferrer et al., 2017), it is possible that the translating supra-canopy may deform so that the obstruction may be fully or partly overcome (e.g. Fig 1b). Alternatively, under some circumstances salt may inflate to allow sediments to rise and translate across obstructions (e.g. Dooley et al., 2017; 2018l Ferrer et al., 2017). We therefore suggest that negative relief is more likely to be a permanent obstruction than positive relief if a minibasin subsides deeply into it.

Third and finally, in the Gulf of Mexico the pattern of supra-canopy strain becomes more complex with time, becoming compartmentalized into series of flow cells (*sensu* Peel et al., 1995) as minibasins weld to the base-of-salt and become obstructed. This contrasts with the system described in Ferrer et al (2017) in which strain patterns simplify with time. In that study, highs on the slope result in initial partitioning of strain into sub-systems. However, once enough salt accumulates upslope of the high such that the high becomes overthrust, the system may subsequently revert to a single gravitational extensional-contractional system of regional extent.

8. Concluding Remarks

We aimed to explain the complex distribution of supra-canopy extension and shortening observed in an array of minibasins located in the lower slope of the northern Gulf of Mexico. We found that

where minibasins are of sufficient thickness, they interact with and weld to a rugose base-of-salt. Welding impacts the translation potential of these minibasins, either by stopping them completely or slowing them down, depending on the severity of the obstruction. The obstruction of a given minibasin, in combination with continued downslope motion of the salt and the surrounding overburden, typically results in zones of shortening immediately upslope of the obstructed minibasin and extensional immediately downslope. Thus, obstructed minibasins exert a major control on patterns of supra-canopy strain and may result in a strain pattern that is decidedly more complex than that observed in salt-detached slopes translating above a smooth base-of-salt.

By assessing whether a minibasin is obstructed, and if so, to what degree, we may be able to understand the relative movement histories of minibasins in a given province, and in fact, predict how a minibasin is moving today. This is valuable for two main reasons. First, if we can understand the likely minibasin kinematics associated with obstruction, we have a conceptual framework within which to explain the complex map-view strain fields. Thus, we can make sense of the geometry, kinematics and distribution of faults, folds and welds in and around obstructed minibasins, aiding structural restorations. Second, being able to predict present-day minibasin kinematics may help those drilling boreholes in minibasin provinces to predict likely stress fields and thus the stability and lifetime of well bores (e.g. Tingay et al., 2011; King et al., 2012).

In summary, this study has demonstrated the importance of obstructed minibasins and the influence they can have upon supra-salt strain patterns. It is likely that the process of minibasin obstruction causes predictable spatial and temporal changes in seafloor topography that control the location and character of depositional systems, and hence reservoir distribution in other minibasin provinces. Concepts outlined in this article are applicable to other salt basins where minibasins are

translating downslope in the presence of significant base-of-salt relief (e.g. North Sea, Gulf of Mexico, South Atlantic margins, Scotian margin, offshore Morocco).

9. Acknowledgements

We would like to thank Nancy Cottington for figure drafting. We thank Martin Jackson and Scot Krueger for scientific discussions in the early stages in this work that helped us clarify our thoughts. We also thank Gillian Apps and Juan Soto for scientific discussions. Thanks to CGG and WesternGeco Multiclient for providing the 3D seismic data and to the Bureau of Ocean Energy Management for seafloor imagery. The project was funded by the Applied Geodynamics Laboratory (AGL) Industrial Associates program, comprising the following companies: Anadarko, Aramco Services, BHP Billiton, BP, CGG, Chevron, Condor, EcoPetrol, EMGS, ENI, ExxonMobil, Hess, Ion-GXT, Midland Valley, Murphy, Nexen USA, Noble, Petrobras, Petronas, PGS, Repsol, Rockfield, Shell, Spectrum, Equinor, Stone Energy, TGS, Total, WesternGeco, and Woodside (http://www.beg.utexas.edu/agl/sponsors). The authors received additional support from the Jackson School of Geosciences, The University of Texas at Austin. Publication authorised by the Director, Bureau of Economic Geology, The University of Texas at Austin.

10. Figure Captions

Figure 1. (a) Schematic model of a salt-detached slope system with a smooth base-of-salt. Note the simple extension-translation-contraction structural zonation (modified from Rowan et al., 2004). (b) Sketch of a physical model (modified from Ferrer et al., 2017) showing the structural styles developed when a mid-slope seamount fully protrudes above top salt at the onset of gliding. Note how the slope system is partitioned into two extensional-contractional subsystems either side of the seamount. (c) Schematic model of a salt-detached slope system where a prekinematic overburden of uniform thickness is passively-translated across a base-of-salt high block ('step-up/step-down' scenario shown although 'step-down/step-up' scenarios also occur). Key processes influencing local strains are shown at an early-stage (i) and a late-stage (ii) (modified from Dooley et al. 2017, see paper for more details). On the updip side of the high block a flux mismatch causes salt to thicken. This reduces the effects of basal drag, such that salt velocity increases through time. This eventually causes extension as the overburden and salt pull away from the thickened salt. On the downdip side of the high block, a flux mismatch initially results in rapid extension. This extension is facilitated by the absence of a buttress and the proximity of the open toe. Extensional structures formed on the high block are amplified as they translate through an extensional hinge and shorten as they translate through a compressional hinge.

Figure 2. Seafloor bathymetry map of the northern Gulf of Mexico and the Sigsbee Canopy. The study area is located in the mid-to-lower slope. Bathymetry map sourced from the Bureau of Ocean

Energy Management. Black lines show offshore protraction areas. Inset shows broader geographical location of bathymetry data.

Figure 3. Schematic regional representation of key elements of the deep water Northern Gulf of Mexico (modified from Pilcher et al (2011). Feeders between the primary minibasins allowed deep Louann salt to rise and form the shallow Sigsbee canopy, into which the supra-salt minibasins (yellow) have subsided. Welds are indicated by paired red dots. The red and purple lines indicate what we have mapped and termed the base Sigsbee Canopy surface (shown in map-view in Figure 4a) and the top Sigsbee Canopy surface (shown in map-view in Figure 4b), respectively. Note the rugosity of the base Sigsbee Canopy surface and that for the purposes of this study, the surface extends down the feeders.

Figure 4. (a) Map view of the highly-rugose base Sigsbee Canopy surface. Purple areas are feeders and reds show base-of-salt highs (b) Map view of the top Sigsbee Canopy surface, each structural low hosts a minibasin that has subsided into the Sigsbee canopy

Figure 5. Seismic cross-sections showing representative examples of features used to classify the predominant strain in a given area. (a and b) evidence of extensional faults in the supra-canopy indicate extensional strain. (c) folding, (d) thrusting, and (e and f) secondary welding (squeezed diapir) all indicate shortening.

Figure 6. Map view of distribution of extensional and shortening strains in the supra-canopy shown above a grayscale view of the top Sigsbee Canopy surface. Note the patchy and complex distribution of extension and shortening. Importance of locations A-E are discussed in the text.

Figure 7. Schematic diagram showing the concept of minibasin obstruction. At an early stage (a) the minibasins are translating downslope but are too thin to interact with the base-of-salt relief. At a later stage (b), the central minibasin has subsided deep enough that it welds against the base-of-salt. The minibasin is then obstructed from translating downslope and the freely-translating minibasin further upslope runs into the back of the obstructed minibasin. This creates a zone of shortening. In contrast, the unobstructed minibasin and salt further downslope continues moving freely downslope, pulling away from the obstructed minibasin and creating an extensional breakaway.

Figure 8. (a-d) Overhead views showing the evolution of the top surface of a physical model of minibasin obstruction (see appendix 1 for model setup information). (a) Minibasin 1 and Minibasin 2 are translating downslope, updip of a base-of-salt ramp. (b) Minibasin 1 moves closer to the ramp, feels the effect of the ramp, and slows down. Minor shortening occurs to its upslope flank as Minibasin 2 continues to move downslope more rapidly. (c) Minibasin 1 is now welded to the base-of-salt ramp and is therefore an obstructed minibasin. A well-developed fold-and-thrust belt develops upslope of obstructed Minibasin 1 whereas an extensional breakaway develops to its downslope. (d) At a much later stage in the evolution of the model Minibasin 1, which was previously welded to, and obstructed by, the base-of-salt ramp, has translated further down dip, suggesting that mildly- to moderately-obstructed minibasins can still translate downslope once thy

have welded to the base-of-salt. (e) Strain map of the top model surface after 42 hours showing 2D strains in E-W direction. Note the marked shortening strains located updip of the obstructed minibasin and the extensional strains downdip of the obstructed minibasin. The model setup is documented in the appendix.

Figure 9. Vertical cross-sections taken from the physical model shown in Figure 8. The locations of the cross-sections are shown in Fig 8d. Note how MB-1 is welded to the base-of-salt and thus obstructed. Folds and thrusts (i.e. shortening features) are observed upslope of the obstructed minibasin and extensional features are observed immediately downslope.

Figure 10. Seismic cross-sections showing uninterpreted and interpreted examples of obstructed minibasins i.e. where the bases of supra-canopy minibasins have subsided deep enough that they have welded to the base Sigsbee Canopy surface. (a) Minibasin has subsided into a major feeder (severely-obstructed minibasin). (b) Minibasin welded to, and obstructed by, a steeply-dipping high in the base-of-salt (highly-obstructed minibasin). (c) Minibasin welded to, and obstructed by, a moderately-dipping high in the base-of-salt (moderately-obstructed minibasin). (d) Minibasin welded to, and obstructed by, a gently landward-dipping base-of-salt (mildly-obstructed minibasin).

Figure 11. Map view showing the number, size and distribution of obstructed minibasins shown above a grayscale top Sigsbee salt surface map.

Figure 12. Map view showing distribution of obstructed minibasins as well as areas of extensional and shortening strains. Note how many obstructed minibasins are associated with a zone of shortening immediately to the upslope and shortening to the immediate downslope. Locations 1-9 are clear examples of where obstructed minibasins show shortening strains to their immediate upslopes and extensional strains to their immediate downslopes.

Figure 13. Map view showing the outlines of obstructed minibasins in the study area shown above a grayscale top Sigsbee salt surface map. Obstructed minibasins that show upslope shortening and downslope extension are coloured red, whereas those that does not display upslope shortening and downslope extension are coloured blue. Importance of location W is discussed in the text.

Figure 14. Map view showing the outlines of obstructed minibasins shown above a grayscale top Sigsbee salt surface map. Polygons are colour-coded according to the degree to which they are obstructed. Importance of locations X, Y, Z are discussed in the text.

Figure 15. Schematic model of a salt-detached slope system above a rugose base-of-salt surface where the supra-canopy stratigraphy is in the form of multiple subsiding minibasins that are translating downslope. (a) early-stage configuration where minibasin bases have not subsided deep enough to interact and weld against the rugose base-of-salt. A simple three-division structural zonation of the slope occurs. (b) late-stage configuration where the minibasins have subsided deep enough to interact and weld with the rugose base-of-salt. There are varying degrees of obstruction (red = severe obstruction; orange = high degree of obstruction; yellow = moderate obstruction;

green = mild obstruction) and a number of extensional-contractional gravitational sub-systems or 'flow cells' form between obstructed minibasins.

Caption for Appendix Figure A1. Overhead view showing the set up for the physical model of minibasin obstruction, the results of which are shown in Figures 8 and 9 and discussed in the text (see Appendix 1 for details).

Appendix 1: Physical model set up, materials and data capture

As is common for physical models of salt tectonics, we simulated our salt layer using ductile silicone polymer (polydimethylsiloxane [PDMS], trade named SGM36; Weijermars, 1986) and its siliciclastic overburden using brittle, dry, granular materials consisting of quartz sands and ceramic microspheres. A 3-cm-thick silicone layer formed our canopy analog and this pinched out against a left-dipping base-salt ramp (Figure A1). Two circular minibasins with a diameter of 15 cm were emplaced on the model surface as mounded positive reliefs in the positions shown in Figure A1. To ensure the minibasins formed bowl-shaped depressions the density of the minibasin "fill" was altered from the center to the periphery of the initial mounds. The central core of the minibasin was 1.4 times that of our salt analog, and the periphery of the minibasin was the same density as our salt analog. This density ratio was achieved by varying the proportions of silica sands and ceramic microspheres in the brittle overburden (see Dooley et al., 2009; for further details). Minibasin 1 was sunk to 2.5 cm, and Minibasin 2 was sunk to a depth of 2 cm (orange and yellow

layers in Figure 8) before the entire model (blue surface shown in Figure 7; purple, grey and blue layers in Figure 8) surface was covered in a 1-cm-thick sand and microsphere mixture. Gravity gliding was initiated by simply tilting the rig to the right to a dip of 4° (Figure A1), reducing the effective dip of the base-salt ramp on the right to 6°.

Computer-controlled cameras photographed the obliquely lit upper surface of the models at set time intervals. These photographs of the surface of the model are shown in Figure 8a-d. These images were also processed in 2D by a DIC (digital image correlation) software system (DaVis by LaVision) generating the strain map shown in Figure 8e. For more details on DIC monitoring and processing techniques, see Adam et al. (2005). The completed model was set using a gelatin mixture and sliced at intervals of 3 mm generating the section views shown in Figure 9.

11. References

Allen, H., Jackson, C.A.-L. & Fraser, A.J. (2016) Gravity-Driven Deformation of a Youthful Saline Giant: The Interplay between Gliding and Spreading in the Messinian Basins of the Eastern Mediterranean. *Petroleum Geoscience*, **22,** 340-356.

Bouroullec, R. & Weimer, P. (2017) Geometry and Kinematics of Neogene Allochthonous Salt Systems in the Mississippi Canyon, Atwater Valley, Western Lloyd Ridge, and Western Desoto Canyon Protraction Areas, Northern Deep-Water Gulf of Mexico. *AAPG Bulletin*, **101,** 1003-1034.

Brun, J.-P. & Fort, X. (2004) Compressional Salt Tectonics (Angolan Margin). *Tectonophysics*, **382,** 129-150.

Brun, J.-P. & Fort, X. (2011) Salt Tectonics at Passive Margins: Geology Versus Models. *Marine and Petroleum Geology*, **28,** 1123-1145.

Buffler, R.T. (1991) Early Evolution of the Gulf of Mexico Basin.

Carter, R.C., Gani, M.R., Roesler, T. & Sarwar, A.K. (2016) Submarine Channel Evolution Linked to Rising Salt Domes, Gulf of Mexico, USA. *Sedimentary Geology*, **342,** 237-253.

Cobbold, P. & Szatmari, P. (1991) Radial Gravitational Gliding on Passive Margins. *Tectonophysics*, **188,** 249-289.

Curry, M.A., Peel, F.J., Hudec, M.R. & Norton, I.O. (2018) Extensional Models for the Development of Passive-Margin Salt Basins, with Application to the Gulf of Mexico. *Basin Research*, **30,** 1180-1199.

Diegel, F.A., Karlo, J., Schuster, D., Shoup, R. & Tauvers, P. (1995) Cenozoic Structural Evolution and Tectono-Stratigraphic Framework of the Northern Gulf Coast Continental Margin.

569 Dooley, T.P., Jackson, M.P. & Hudec, M.R. (2009) Inflation and Deflation of Deeply Buried Salt Stocks During
570 Lateral Shortening. *Journal of Structural Geology*, **31,** 582-600.
571 Dooley, T.P. & Hudec, M.R. (2017) The Effects of Base of salt Relief on Salt Flow and Suprasalt Deformation
572 Patterns—Part 2: Application to the Eastern Gulf of Mexico. *Interpretation*, **5,** SD25-SD38.
573 Dooley, T., Hudec, M., Carruthers, D., Jackson, M. & Luo, G. (2017) The Effects of Base of salt Relief on Salt
574 Flow and Suprasalt Deformation Patterns—Part 1: Flow across Simple Steps in the Base of salt:
575 Interpretation, 5, This Issue, Doi: Http://Dx. Doi. Org/10.1190, INT-2016-0088.1.
576 Dooley, T.P., Hudec, M.R., Pichel, L.M. & Jackson, M.P.A. (2018) The Impact of Base of salt Relief on Salt Flow
577 and Suprasalt Deformation Patterns at the Autochthonous, Paraautochthonous and
578 Allochthonous Level: Insights from Physical Models. *Geological Society, London, Special*
579 *Publications*, **476,** SP476. 413.
580 Duffy, O.B., Fernandez, N., Hudec, M.R., Jackson, M.P., Burg, G., Dooley, T.P. & Jackson, C.A.-L. (2017) Lateral
581 Mobility of Minibasins During Shortening: Insights from the SE Precaspian Basin, Kazakhstan.
582 *Journal of Structural Geology*.
583 Duffy, O.B., Dooley, T.P., Hudec, M.R., Jackson, M.P., Fernandez, N., Jackson, C.A-L. & Soto, J.I. (2018) Structural
584 Evolution of Salt-Influenced Fold-and-Thrust Belts: A Synthesis and New Insights from Basins
585 Containing Isolated Salt Diapirs. *Journal of Structural Geology*, **114,** 206-221.
586 Fernandez, N., Duffy, O.B., Peel, F.J., Hudec, M.R. (XXXX) Influence of Minibasin Obstruction on Regional
587 Canopy Dynamics in the Northern Gulf of Mexico. *In review* XXXX (companion paper – this will be
588 updated post-review)
589 Ferrer, O., Gratacós, O., Roca, E. & Muñoz, J.A. (2017) Modeling the Interaction between Presalt Seamounts
590 and Gravitational Failure in Salt-Bearing Passive Margins: The Messinian Case in the Northwestern
591 Mediterranean Basin. *Interpretation*, **5,** SD99-SD117.
592 Galloway, W.E., Ganey-Curry, P.E., Li, X. & Buffler, R.T. (2000) Cenozoic Depositional History of the Gulf of
593 Mexico Basin. *AAPG bulletin*, **84,** 1743-1774.
594 Galloway, W.E. (2008) Depositional Evolution of the Gulf of Mexico Sedimentary Basin. *Sedimentary basins*
595 *of the world*, **5,** 505-549.
596 Galloway, W.E., Whiteaker, T.L. & Ganey-Curry, P. (2011) History of Cenozoic North American Drainage Basin
597 Evolution, Sediment Yield, and Accumulation in the Gulf of Mexico Basin. *Geosphere*, **7,** 938-973.
598 Gaullier, V., Brun, J.P., Gue'rin, G. & Lecanu, H. (1993) Raft Tectonics: The Effects of Residual Topography
599 Below a Salt Decollement. *Tectonophysics*, **228,** 363-381.
600 Granado, P., Roca, E., Strauss, P., Pelz, K. & Muñoz, J.A. (2018) Structural Styles in Fold-and-Thrust Belts
601 Involving Early Salt Structures: The Northern Calcareous Alps (Austria). *Geology*.
602 Hudec, M.R. & Jackson, M.P.A. (2004) Regional Restoration across the Kwanza Basin, Angola: Salt Tectonics
603 Triggered by Repeated Uplift of a Metastable Passive Margin. *AAPG Bulletin*, **88,** 971-990.
604 Hudec, M.R., Norton, I.O., Jackson, M.P. & Peel, F.J. (2013) Jurassic Evolution of the Gulf of Mexico Salt
605 Basingulf of Mexico Jurassic Evolution. *AAPG Bulletin*, **97,** 1683-1710.
606 Jackson, M. & Talbot, C.J. (1991) *A Glossary of Salt Tectonics*. Bureau of Economic Geology, University of
607 Texas at Austin.
608 Jackson, C.A.-L., Jackson, M.P. & Hudec, M.R. (2015) Understanding the Kinematics of Salt-Bearing Passive
609 Margins: A Critical Test of Competing Hypotheses for the Origin of the Albian Gap, Santos Basin,
610 Offshore Brazil. *Bulletin*, **127,** 1730-1751.
611 King, R., Backé, G., Tingay, M., Hillis, R. & Mildren, S. (2012) Stress Deflections around Salt Diapirs in the Gulf
612 of Mexico. *Geological Society, London, Special Publications*, **367,** 141-153.
613 Konyukhov, A. (2008) Geological Structure, Evolution Stages, and Petroliferous Complexes of the Gulf of
614 Mexico Basin. *Lithology and Mineral Resources*, **43,** 380-393.
615 Krueger, S.W. (2010) Dynamics of Tear Faults in the Salt-Detached Systems of the Northern Gulf of Mexico.
616 *American Association of Petroleum Geologists Search and Discovery*.

617 Loncke, L., Gaullier, V., Mascle, J., Vendeville, B. & Camera, L. (2006) The Nile Deep-Sea Fan: An Example of
618 Interacting Sedimentation, Salt Tectonics, and Inherited Subsalt Paleotopographic Features.
619 *Marine and Petroleum Geology*, **23,** 297-315.
620 Marton, G. & Buffler, R.T. (1994) Jurassic Reconstruction of the Gulf of Mexico Basin. *International Geology*
621 *Review*, **36,** 545-586.
622 Mondelli, K. (2010) Salt Reconstruction and Study of Depositional History, Upper Jurassic, East Texas Basin,
623 University of Houston.
624 Mount, V., Dull, K., Mentemeier, S., Kennan, L., J. Pindell, & Rosen N. C. (2007) Structural style and evolution of traps
625 in the Paleogene play, deepwater Gulf of Mexico. In *The Paleogene of the Gulf of Mexico and*
626 *Caribbean basins: Processes, events, and petroleum systems: 27th Annual Gulf Coast Section SEPM*
627 *Foundation Bob F. Perkins Research Conference, Houston, Texas*. 54-80.
628 Peel, F.J., Travis, C. & Hossack, J. (1995) Genetic Structural Provinces and Salt Tectonics of the Cenozoic
629 Offshore US Gulf of Mexico: A Preliminary Analysis. *in* M.P.A. Jackson, D.G. Roberts, and S.
630 Snelson, eds., Salt tectonics: a global perspective: *AAPG Memoir* **65**, 153-175.
631 Peel, F.J. (2014) How Do Salt Withdrawal Minibasins Form? Insights from Forward Modelling, and
632 Implications for Hydrocarbon Migration. *Tectonophysics*, **630,** 222-235.
633 Pilcher, R.S., Kilsdonk, B. & Trude, J. (2011) Primary Basins and Their Boundaries in the Deep-Water Northern
634 Gulf of Mexico: Origin, Trap Types, and Petroleum System Implications. *AAPG bulletin*, **95,** 219-
635 240.
636 Pindell, J. & Dewey, J.F. (1982) Permo-Triassic Reconstruction of Western Pangea and the Evolution of the
637 Gulf of Mexico/Caribbean Region. *Tectonics*, **1,** 179-211.
638 Pindell, J.L. (1985) Alleghenian Reconstruction and Subsequent Evolution of the Gulf of Mexico, Bahamas,
639 and Proto-Caribbean. *Tectonics*, **4,** 1-39.
640 Pindell, J.L. & Kennan, L. (2009) Tectonic Evolution of the Gulf of Mexico, Caribbean and Northern South
641 America in the Mantle Reference Frame: An Update. *Geological Society, London, Special*
642 *Publications*, **328,** 1-55.
643 Pindell, J., Graham, R. & Horn, B. (2014) Rapid Outer Marginal Collapse at the Rift to Drift Transition of
644 Passive Margin Evolution, with a Gulf of Mexico Case Study. *Basin Research*, **26,** 701-725.
645 Roca, E., Sans, M. & Koyi, H.A. (2006) Polyphase Deformation of Diapiric Areas in Models and in the Eastern
646 Prebetics (Spain). *AAPG bulletin*, **90,** 115-136.
647 Rowan, M.G. (1995) Structural Styles and Evolution of Allochthonous Salt, Central Louisiana Outer Shelf
648 and Upper Slope. *Jackson MPA, Roberts DG, Snelson S. Salt Tectonics: A Global Perspective*, **65,**
649 199-228.
650 Rowan, M.G., Jackson, M.P. & Trudgill, B.D. (1999) Salt-Related Fault Families and Fault Welds in the
651 Northern Gulf of Mexico. *AAPG bulletin*, **83,** 1454-1484.
652 Rowan, M.G., Peel, F.J. & Vendeville, B.C. (2004) Gravity-Driven Fold Belts on Passive Margins. *in* McClay K.R.
653 ed., Thrust tectonics and hydrocarbon systems: *AAPG Memoir* **82**, 157-182.
654 Rowan, M. (2014) Passive-Margin Salt Basins: Hyperextension, Evaporite Deposition, and Salt Tectonics.
655 *Basin Research*, **26,** 154-182.
656 Salvador, A. (1991) Origin and Development of the Gulf of Mexico Basin. *The Gulf of Mexico basin***,** 389-
657 444.
658 Tew, B.H., Mink, R.M., Mann, S.D., Bearden, B.L. & Mancini, E.A. (1991) Geologic Framework of Norphlet and
659 Pre-Norphlet Strata of the Onshore and Offshore Eastern Gulf of Mexico Area.
660 Tingay, M., Bentham, P., De Feyter, A. & Kellner, A. (2011) Present-Day Stress-Field Rotations Associated with
661 Evaporites in the Offshore Nile Delta. *AAPG Bulletin*, **123,** 1171-1180.
662 Winker, C.D. & Buffler, R.T. (1988) Paleogeographic Evolution of Early Deep-Water Gulf of Mexico and
663 Margins, Jurassic to Middle Cretaceous (Comanchean). *AAPG Bulletin*, **72,** 318-346.

664 Wu, S., Bally, A.W. & Cramez, C. (1990) Allochthonous Salt, Structure and Stratigraphy of the North-Eastern
665 Gulf of Mexico. Part Ii: Structure. *Marine and Petroleum Geology*, **7,** 334-370.
666

667

668

669

670

671

672

673

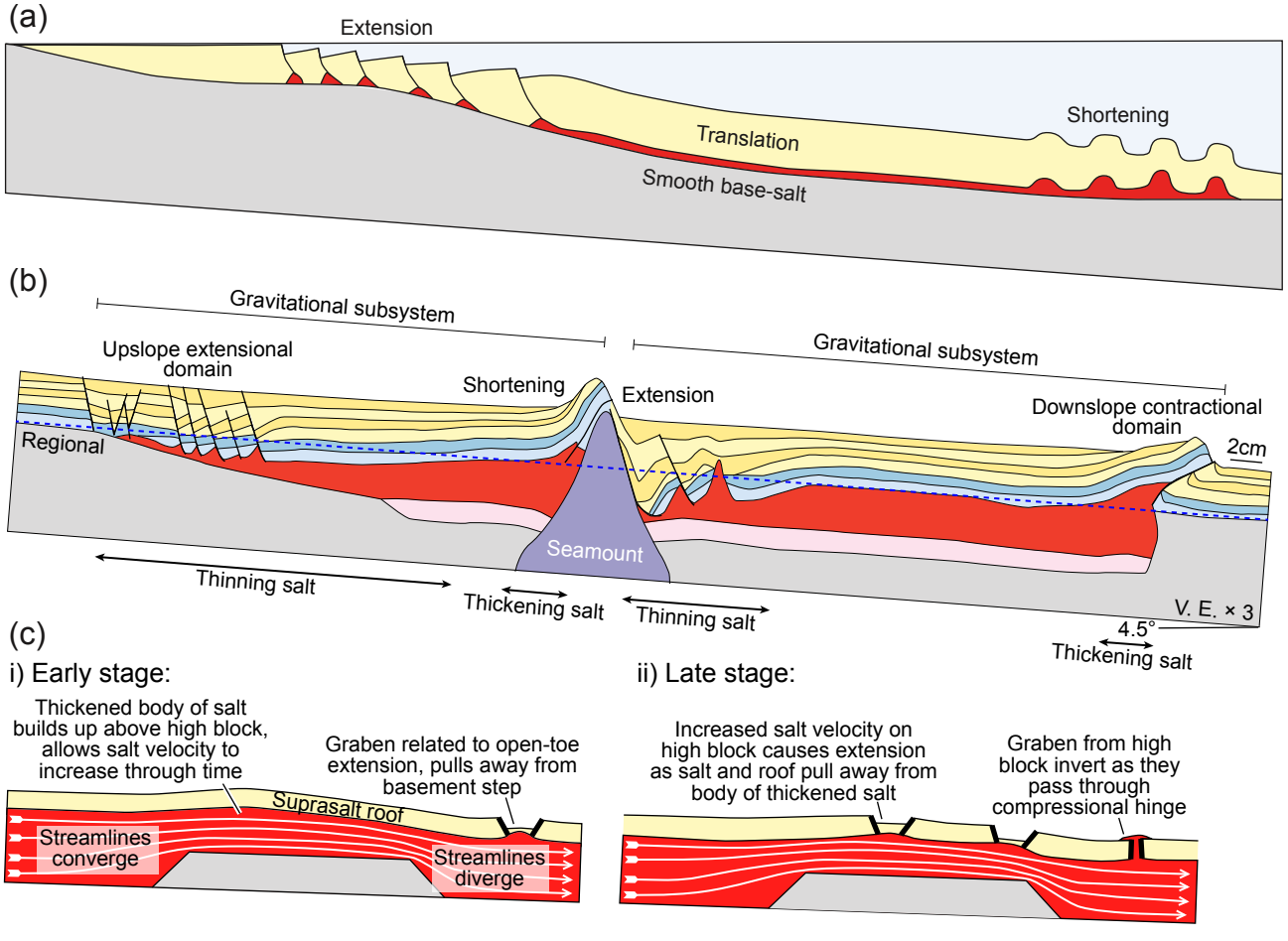
(a)
Extension
Translation
Shortening
Smooth base-salt
(b)
Gravitational subsystem
Upslope extensional domain
Shortening
Extension
Gravitational subsystem
Downslope contractional domain
Regional
2cm
Seamount
Thinning salt
Thickening salt
Thinning salt
V. E. × 3
4.5°
Thickening salt
(c)
i) Early stage:
Thickened body of salt builds up above high block, allows salt velocity to increase through time
Graben related to open-toe extension, pulls away from basement step
Suprasalt roof
Streamlines converge
Streamlines diverge
ii) Late stage:
Increased salt velocity on high block causes extension as salt and roof pull away from body of thickened salt
Graben from high block invert as they pass through compressional hinge

Figure 1

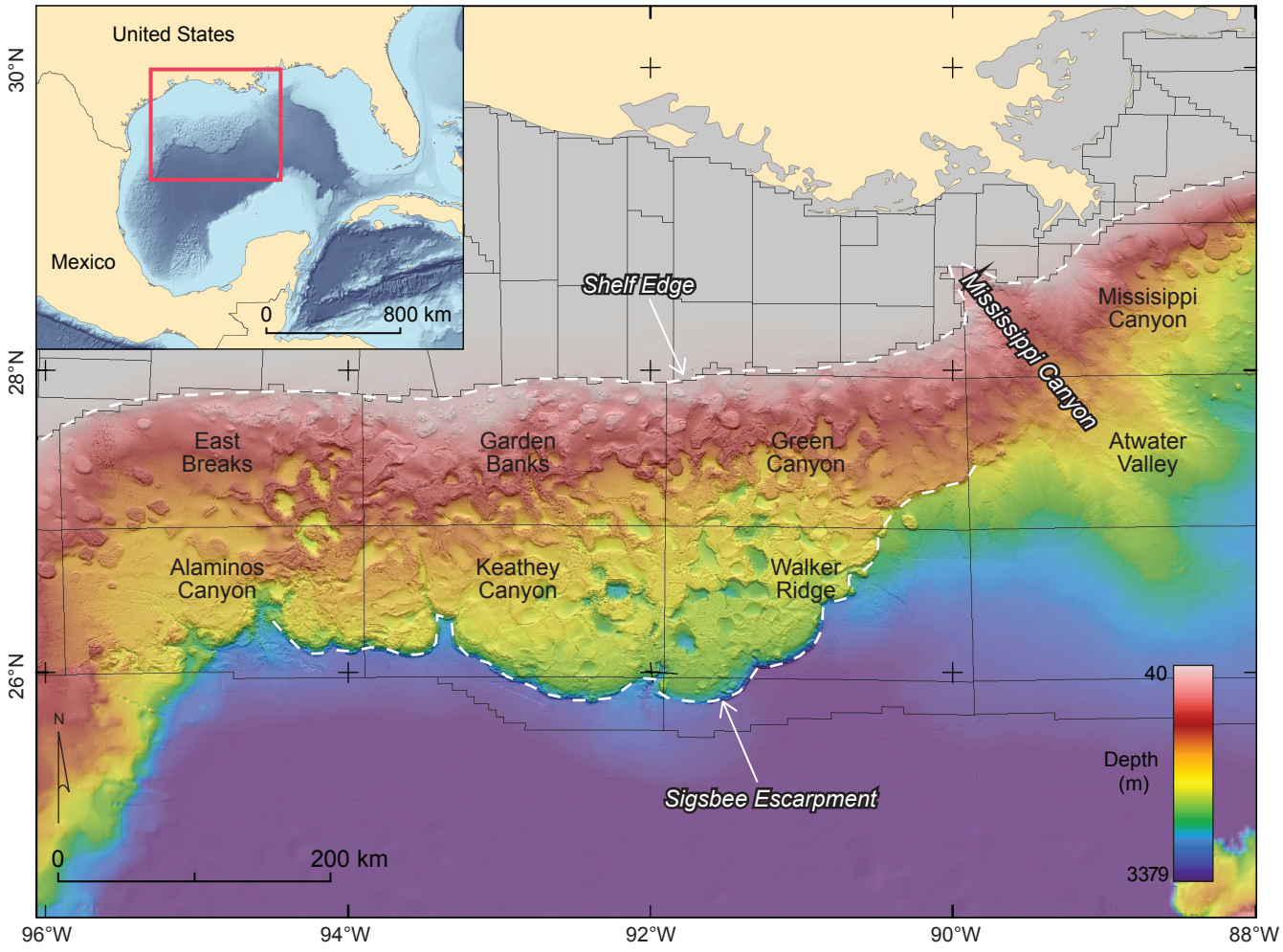
United States
Mexico
0
800 km
Shelf Edge
Mississippi Canyon
Mississippi Canyon
East Breaks
Garden Banks
Green Canyon
Atwater Valley
Alaminos Canyon
Keathey Canyon
Walker Ridge
Sigsbee Escarpment
N
0
200 km
40
Depth (m)
3379
30°N
28°N
26°N
96°W
94°W
92°W
90°W
88°W

Figure 2

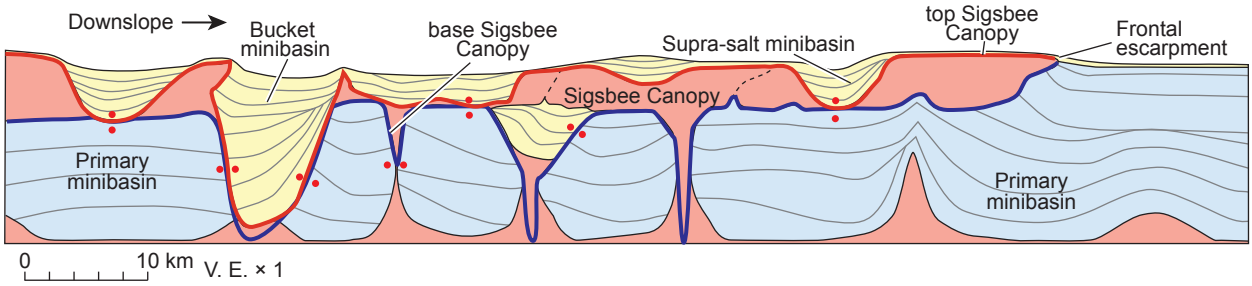
Downslope
Bucket minibasin
base Sigsbee Canopy
Supra-salt minibasin
top Sigsbee Canopy
Frontal escarpment
Sigsbee Canopy
Primary minibasin
Primary minibasin
0
10 km
V. E. × 1

Figure 3

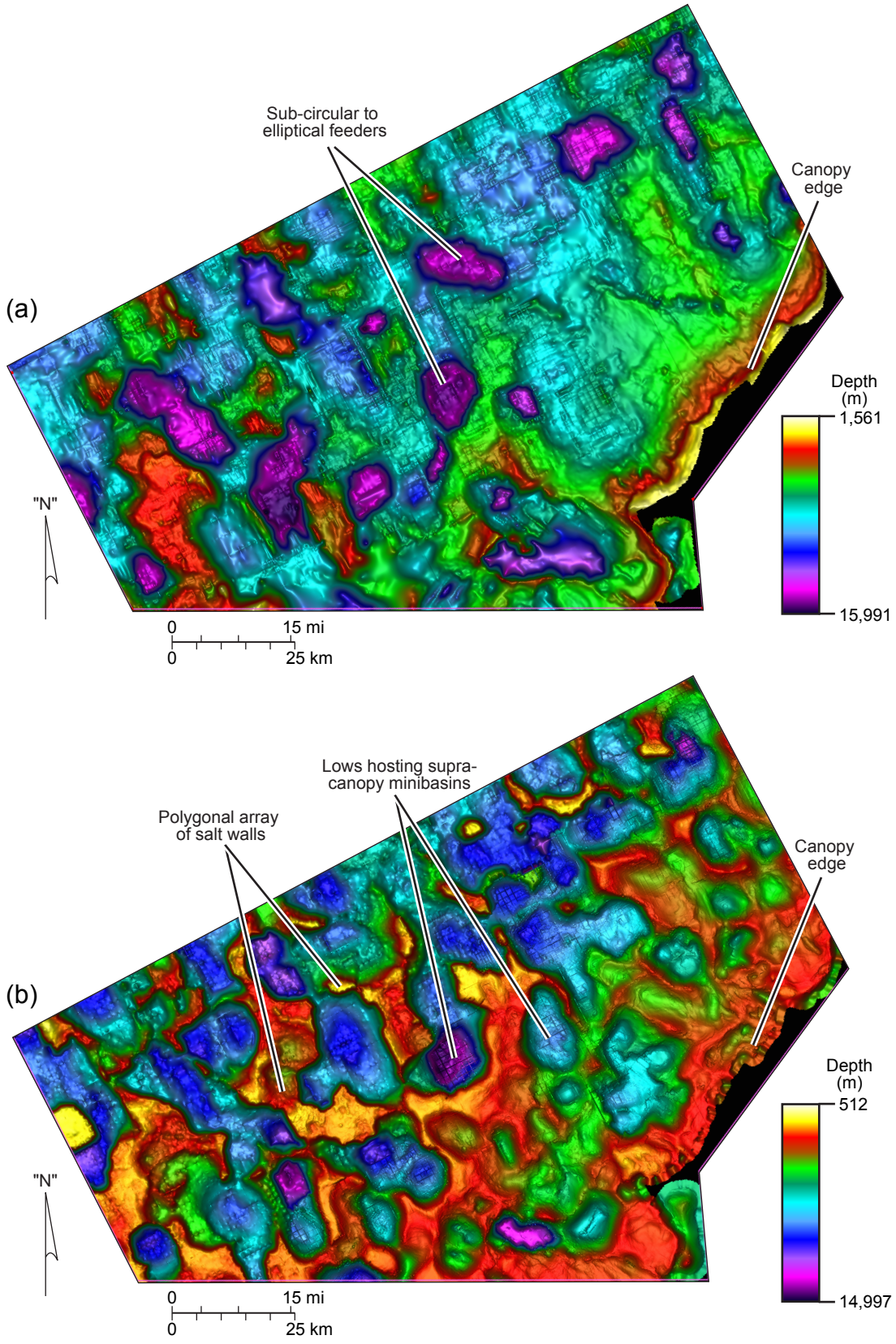
(a)
Sub-circular to elliptical feeders
Canopy edge
Depth (m)
1,561
15,991
"N"
0
15 mi
0
25 km
(b)
Lows hosting supra-canopy minibasins
Polygonal array of salt walls
Canopy edge
Depth (m)
512
14,997
"N"
0
15 mi
0
25 km

Figure 4

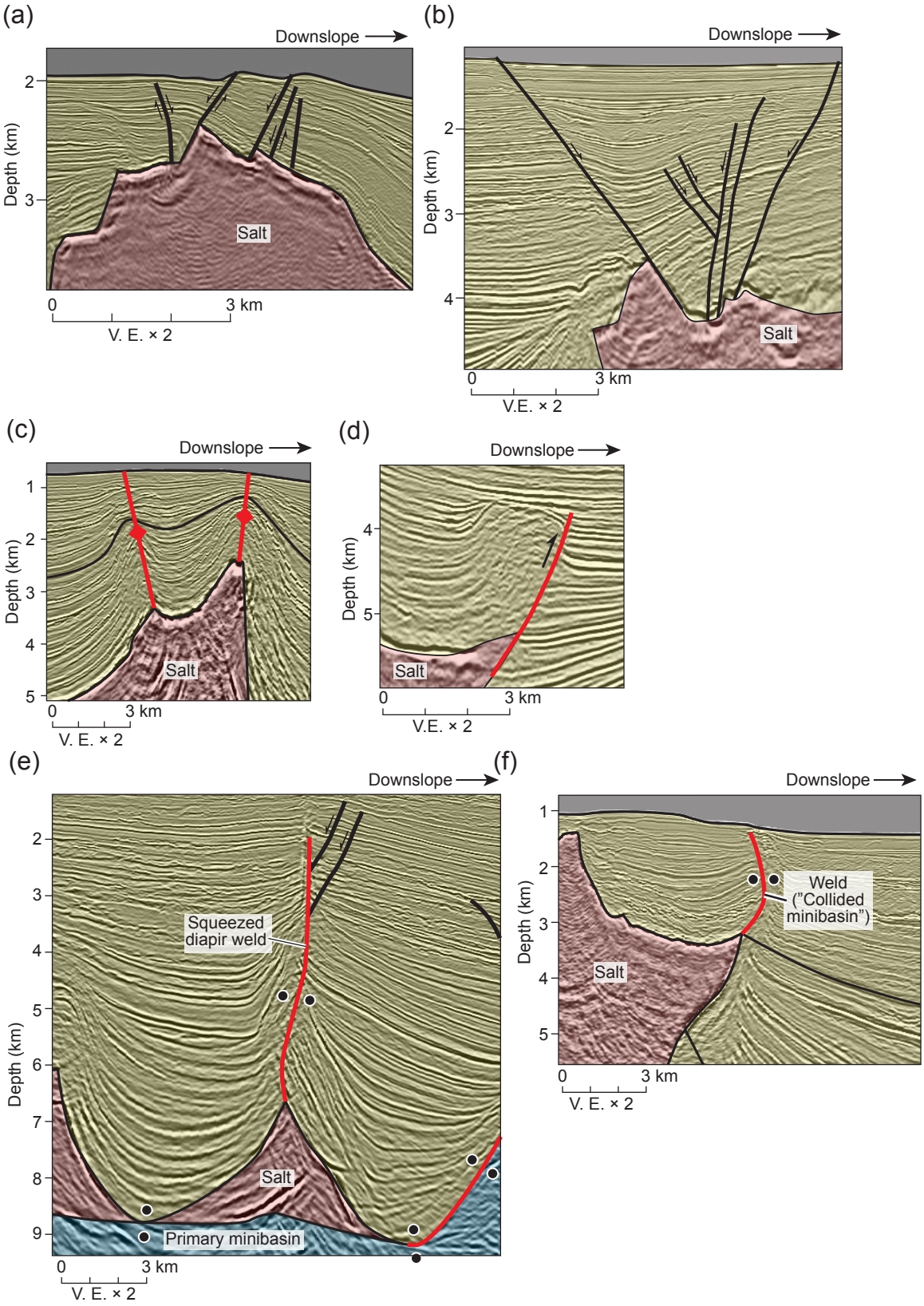
(a)
Downslope
Depth (km)
2
3
Salt
0
3 km
V. E. × 2
(b)
Downslope
Depth (km)
2
3
4
Salt
0
3 km
V.E. × 2
(c)
Downslope
Depth (km)
1
2
3
4
5
Salt
0
3 km
V. E. × 2
(d)
Downslope
Depth (km)
4
5
Salt
0
3 km
V.E. × 2
(e)
Downslope
Depth (km)
2
3
4
5
6
7
8
9
Squeezed diapir weld
Salt
Primary minibasin
0
3 km
V. E. × 2
(f)
Downslope
Depth (km)
1
2
3
4
5
Weld ("Collided minibasin")
Salt
0
3 km
V. E. × 2

Figure 5

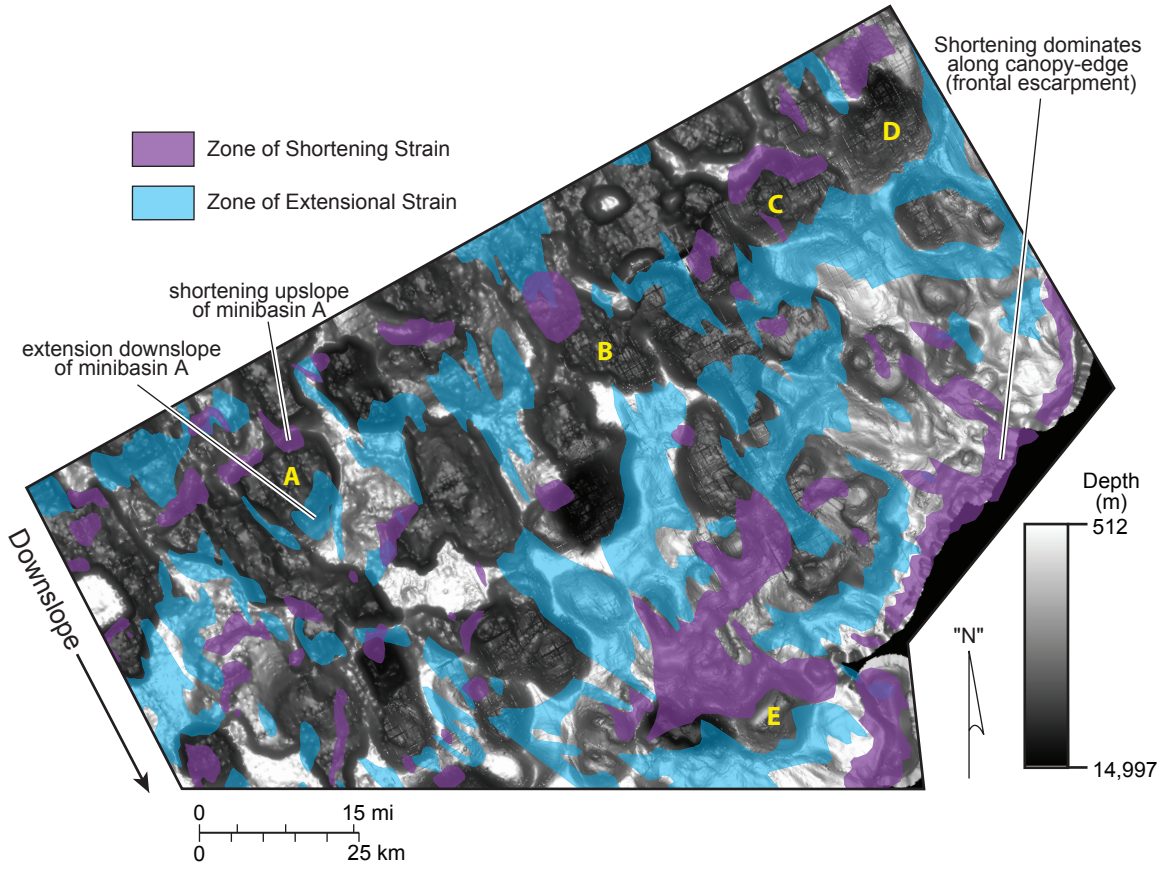
Zone of Shortening Strain
Zone of Extensional Strain
shortening upslope
of minibasin A
extension downslope
of minibasin A
Shortening dominates
along canopy-edge
(frontal escarpment)
A
B
C
D
E
Downslope
"N"
Depth
(m)
512
14,997
0
15 mi
0
25 km

Figure 6

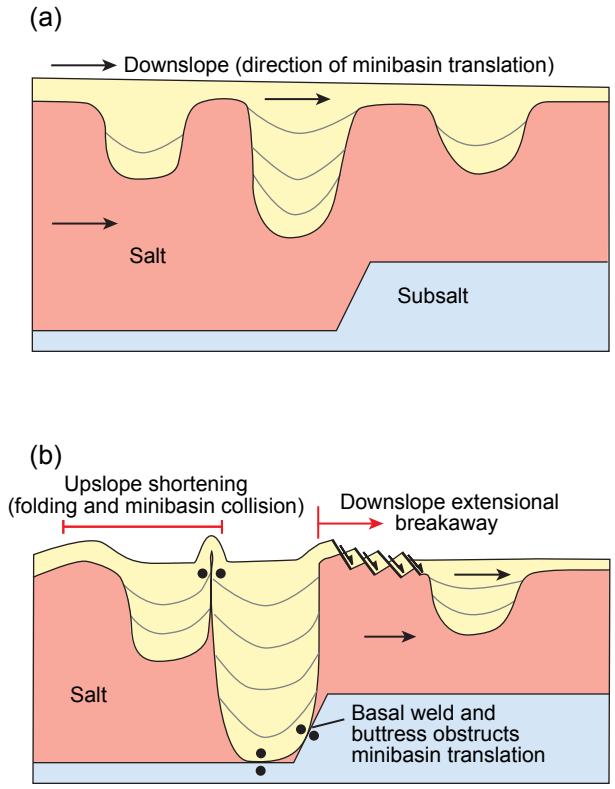
(a)
Downslope (direction of minibasin translation)
Salt
Subsalt
(b)
Upslope shortening
(folding and minibasin collision)
Downslope extensional
breakaway
Salt
Basal weld and
buttress obstructs
minibasin translation

Figure 7

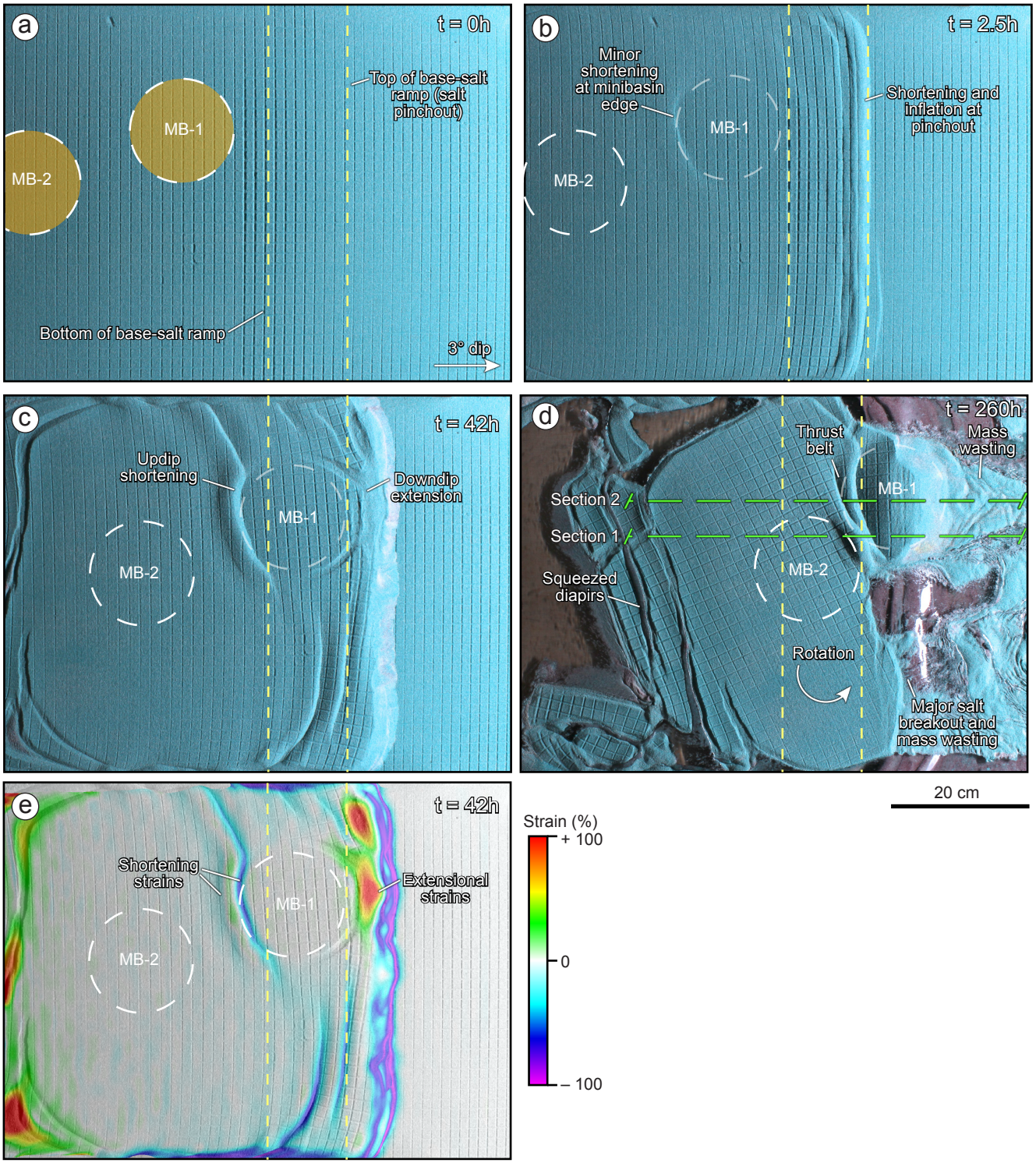
a
t = 0h
MB-1
MB-2
Top of base-salt ramp (salt pinchout)
Bottom of base-salt ramp
3° dip
b
t = 2.5h
Minor shortening at minibasin edge
MB-1
MB-2
Shortening and inflation at pinchout
c
t = 42h
Updip shortening
MB-1
Downdip extension
MB-2
d
t = 260h
Thrust belt
Mass wasting
MB-1
Section 2
Section 1
MB-2
Squeezed diapirs
Rotation
Major salt breakout and mass wasting
20 cm
e
t = 42h
Shortening strains
MB-1
Extensional strains
MB-2
Strain (%)
+ 100
0
– 100

Figure 8

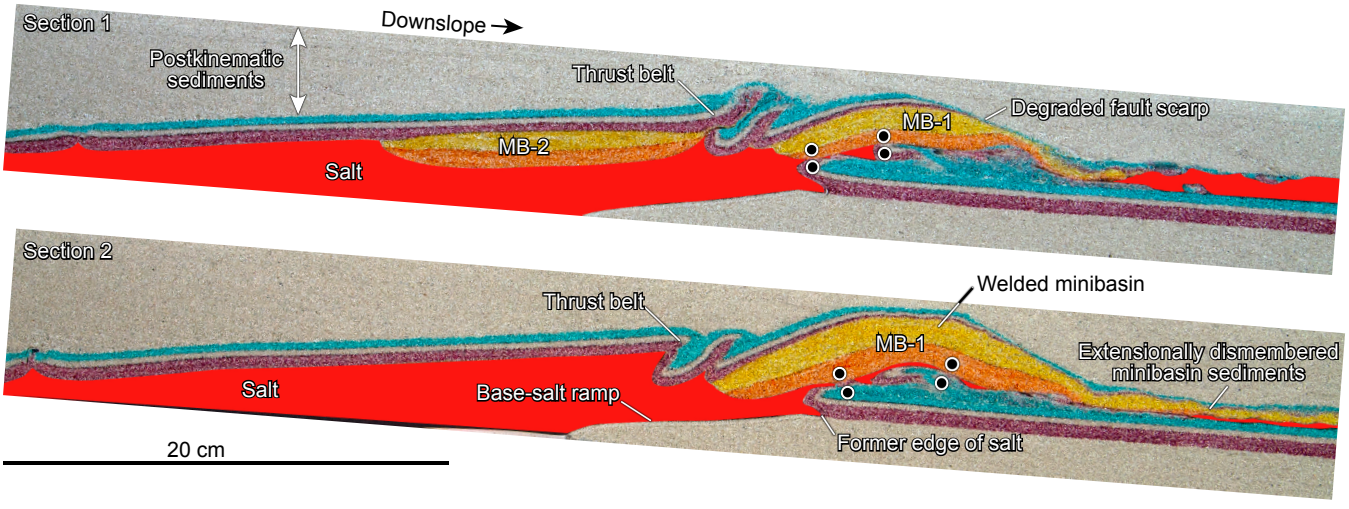
Section 1
Downslope
Postkinematic sediments
Thrust belt
Degraded fault scarp
MB-1
MB-2
Salt
Section 2
Welded minibasin
Thrust belt
MB-1
Extensionally dismembered minibasin sediments
Salt
Base-salt ramp
Former edge of salt
20 cm

Figure 9

Figure10a

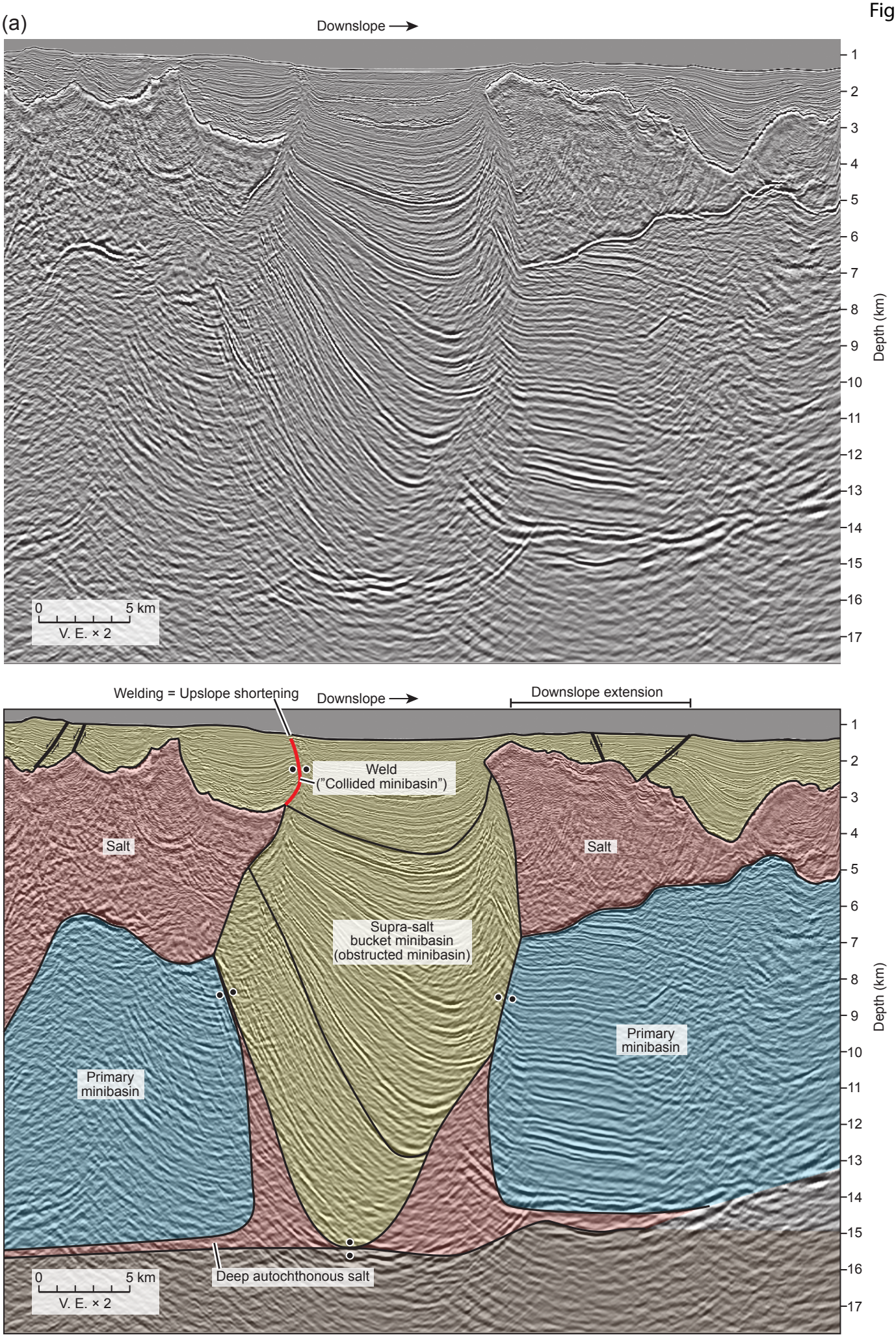
(a)
Downslope
1
2
3
4
5
6
7
8
9
10
11
12
13
14
15
16
17
Depth (km)
0
5 km
V. E. × 2
Welding = Upslope shortening
Downslope
Downslope extension
Weld
("Collided minibasin")
Salt
Salt
Supra-salt
bucket minibasin
(obstructed minibasin)
Primary
minibasin
Primary
minibasin
Deep autochthonous salt
0
5 km
V. E. × 2
1
2
3
4
5
6
7
8
9
10
11
12
13
14
15
16
17
Depth (km)

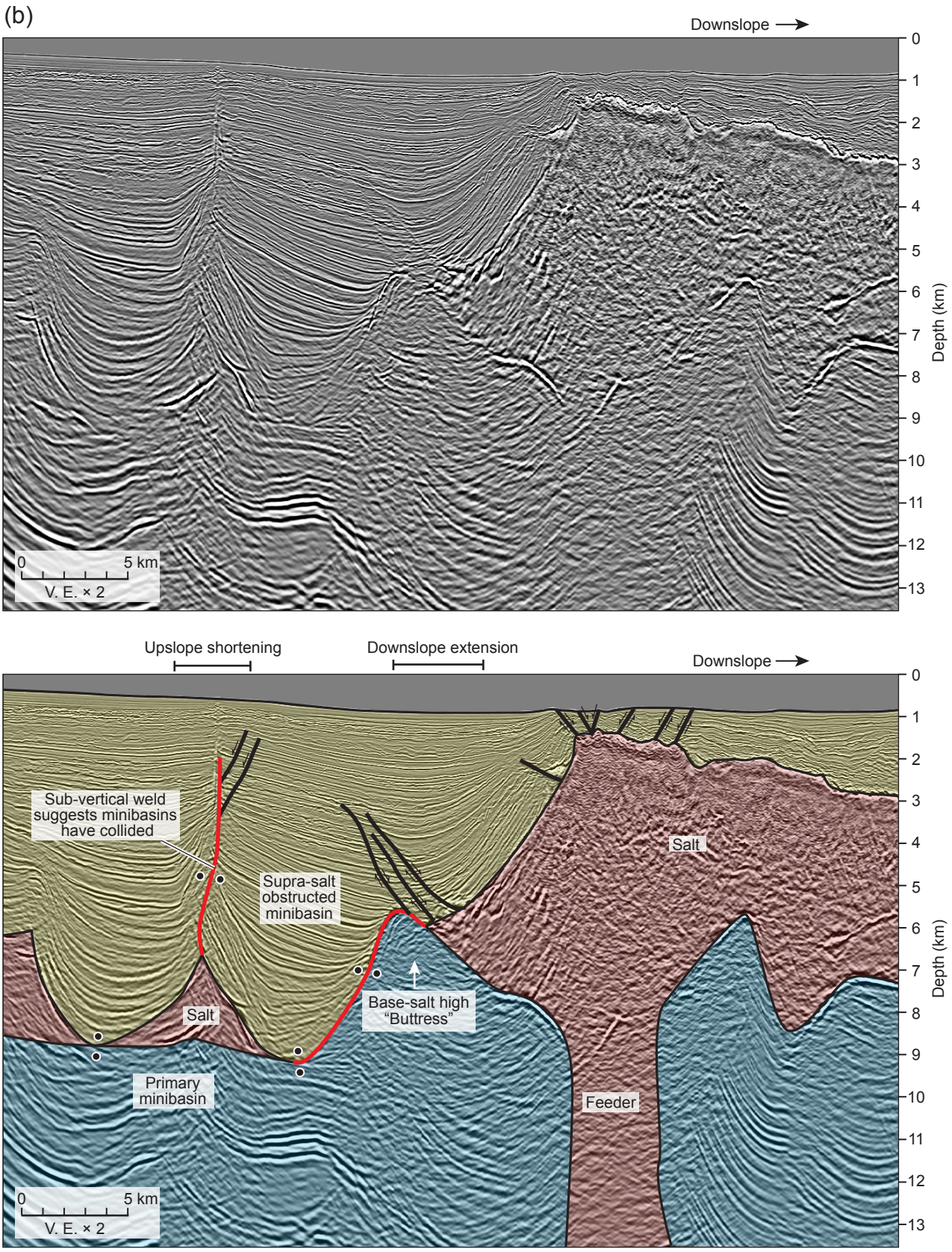
(b)
Downslope
0
1
2
3
4
5
6
7
8
9
10
11
12
13
Depth (km)
0
5 km
V. E. × 2
Upslope shortening
Downslope extension
Downslope
Sub-vertical weld suggests minibasins have collided
Supra-salt obstructed minibasin
Salt
Base-salt high "Buttress"
Salt
Primary minibasin
Feeder
0
5 km
V. E. × 2
Depth (km)

Figure 10b

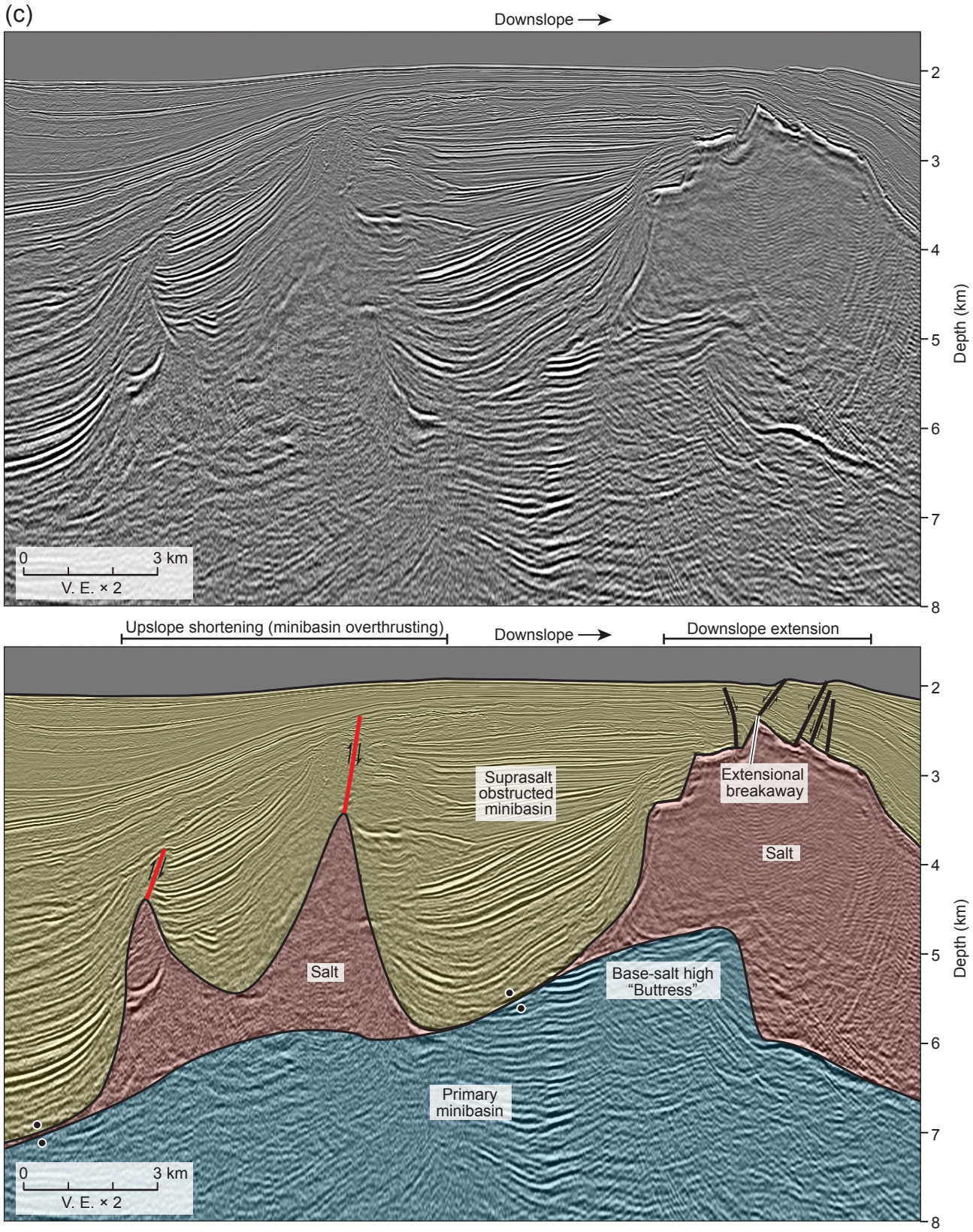
(c)
Downslope
2
3
4
5
6
7
8
Depth (km)
0
3 km
V. E. × 2
Upslope shortening (minibasin overthrusting)
Downslope
Downslope extension
Suprasalt obstructed minibasin
Extensional breakaway
Salt
Salt
Base-salt high "Buttress"
Primary minibasin
0
3 km
V. E. × 2
2
3
4
5
6
7
8
Depth (km)

Figure 10c

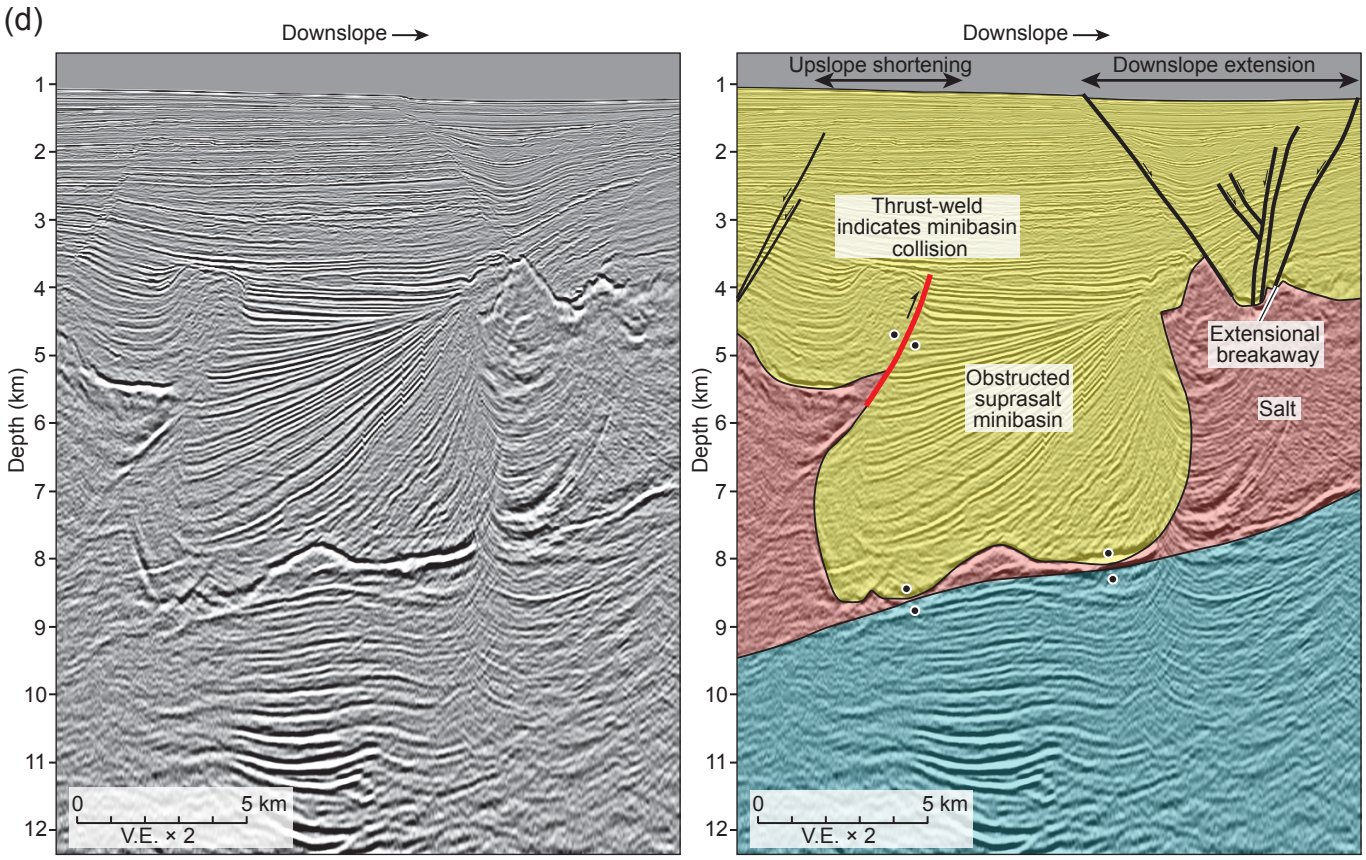
(d)
Downslope
Depth (km)
1
2
3
4
5
6
7
8
9
10
11
12
0
5 km
V.E. × 2
Downslope
Upslope shortening
Downslope extension
Thrust-weld indicates minibasin collision
Extensional breakaway
Obstructed suprasalt minibasin
Salt
Depth (km)
0
5 km
V.E. × 2

Figure 10d

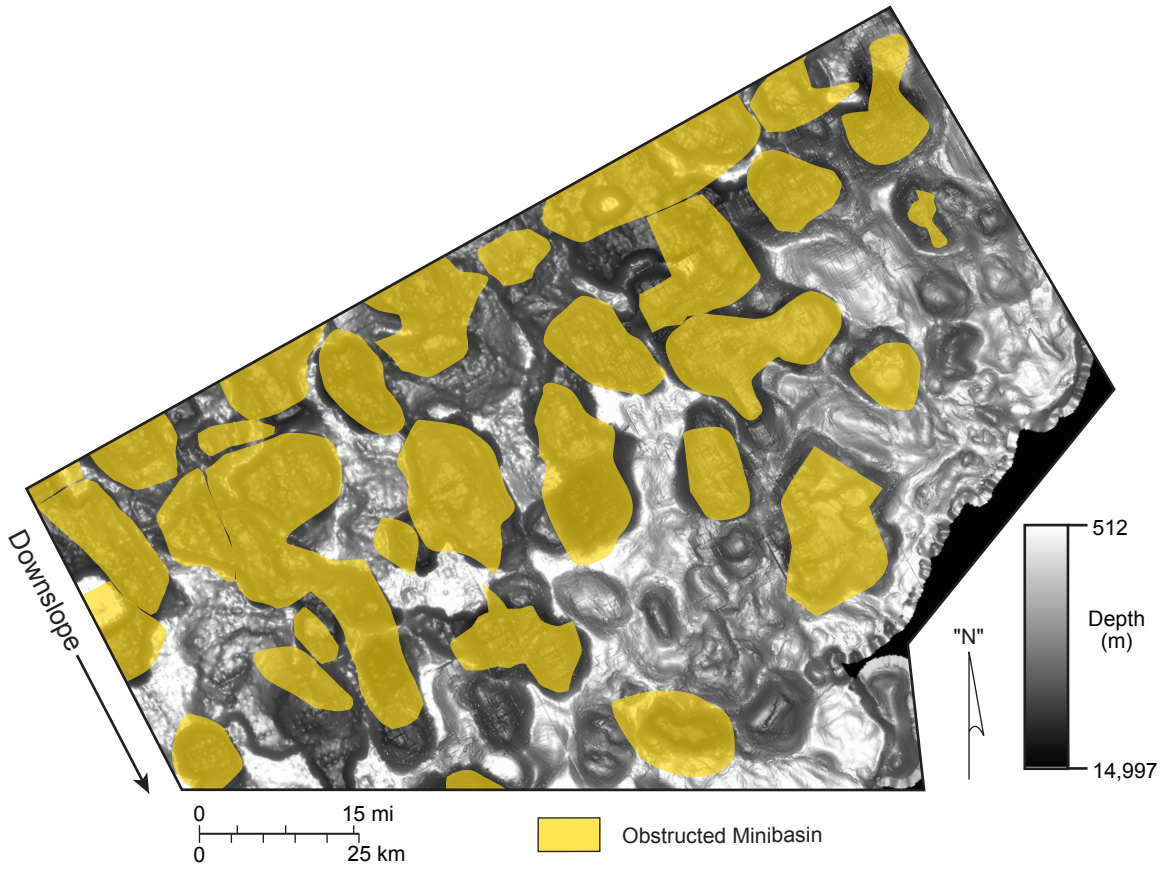
Downslope
"N"
512
Depth
(m)
14,997
0
15 mi
0
25 km
Obstructed Minibasin

Figure 11

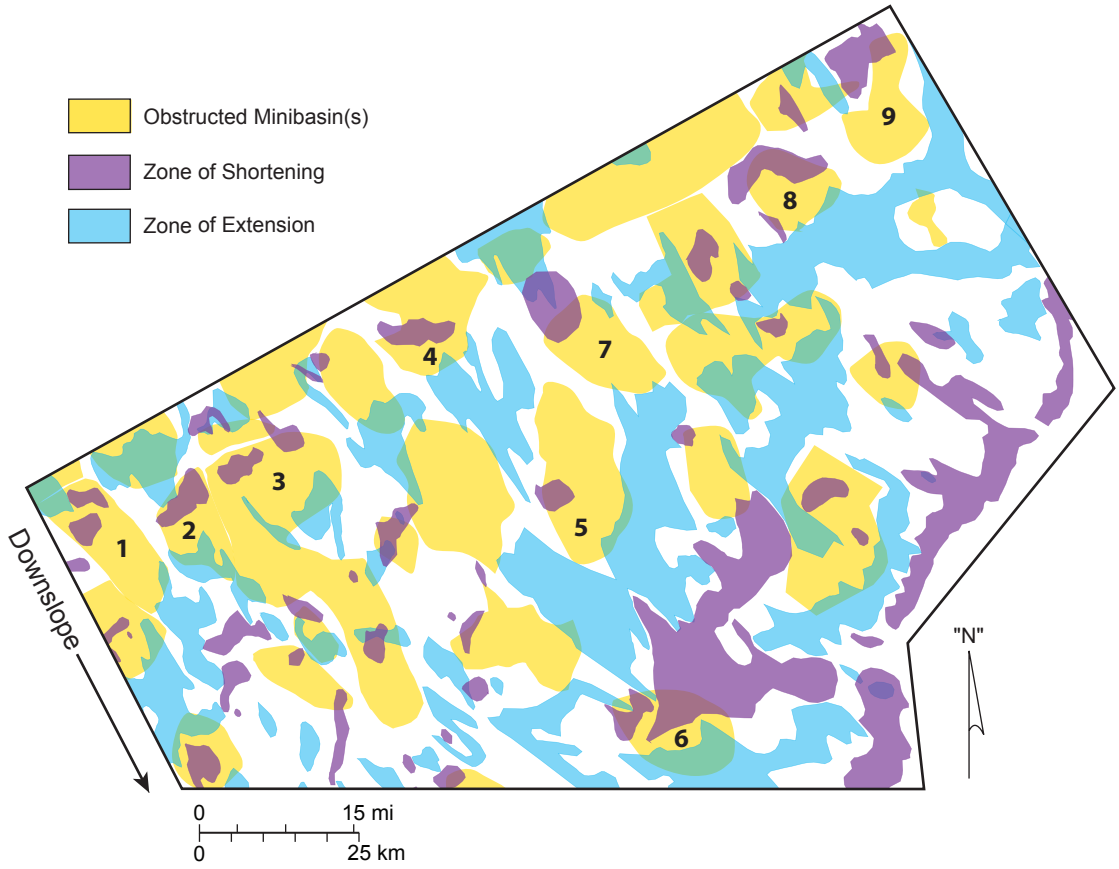
Obstructed Minibasin(s)
Zone of Shortening
Zone of Extension
1
2
3
4
5
6
7
8
9
Downslope
"N"
0
15 mi
0
25 km

Figure 12

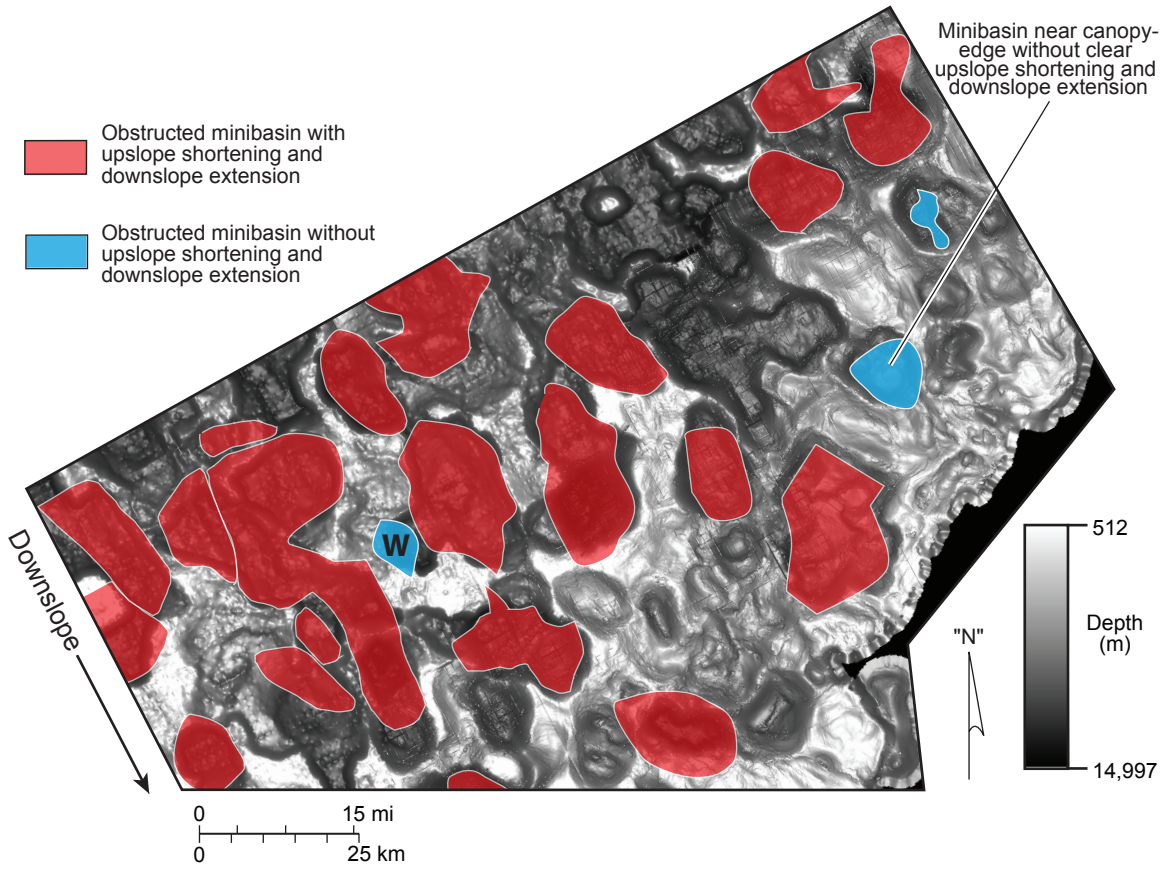
Obstructed minibasin with upslope shortening and downslope extension
Obstructed minibasin without upslope shortening and downslope extension
Minibasin near canopy-edge without clear upslope shortening and downslope extension
W
Downslope
"N"
512
Depth (m)
14,997
0
15 mi
0
25 km

Figure 13

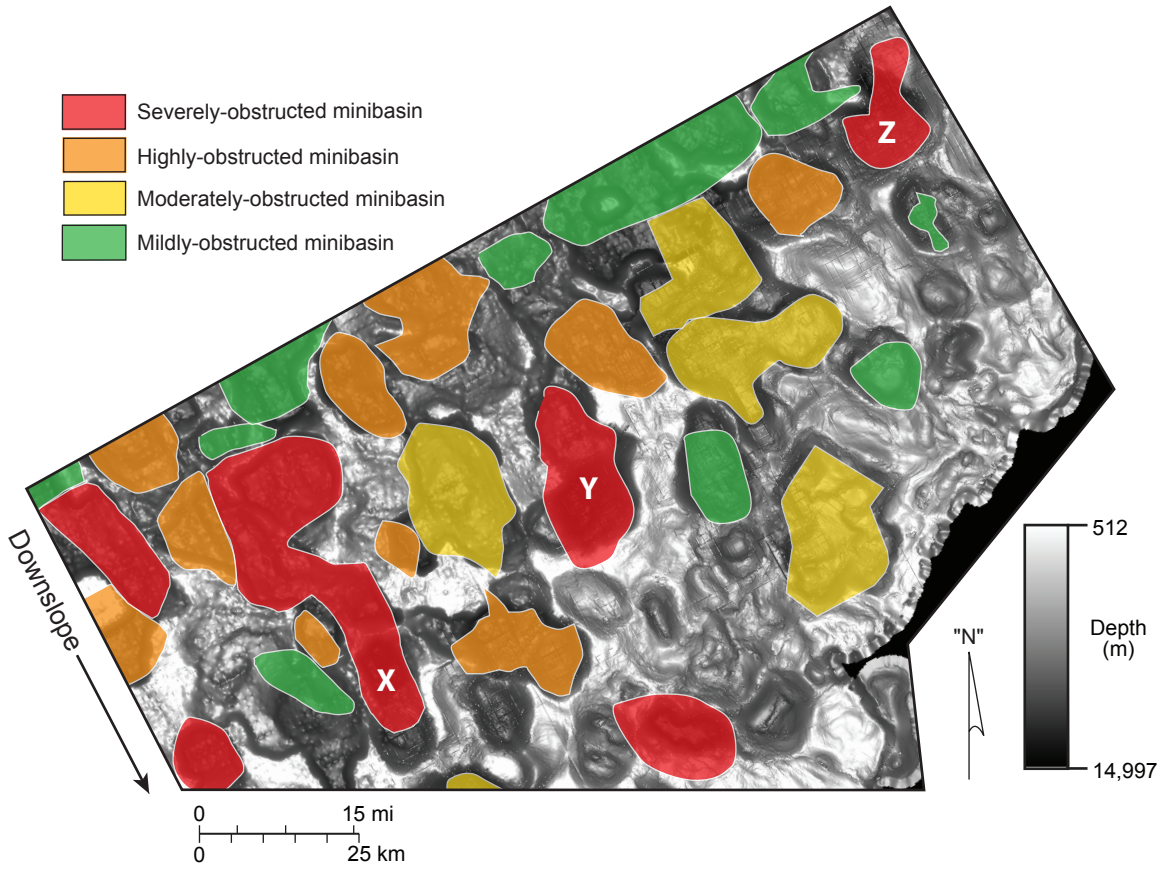
Severely-obstructed minibasin
Highly-obstructed minibasin
Moderately-obstructed minibasin
Mildly-obstructed minibasin
Z
Y
X
Downslope
"N"
512
Depth
(m)
14,997
0
15 mi
0
25 km

Figure 14

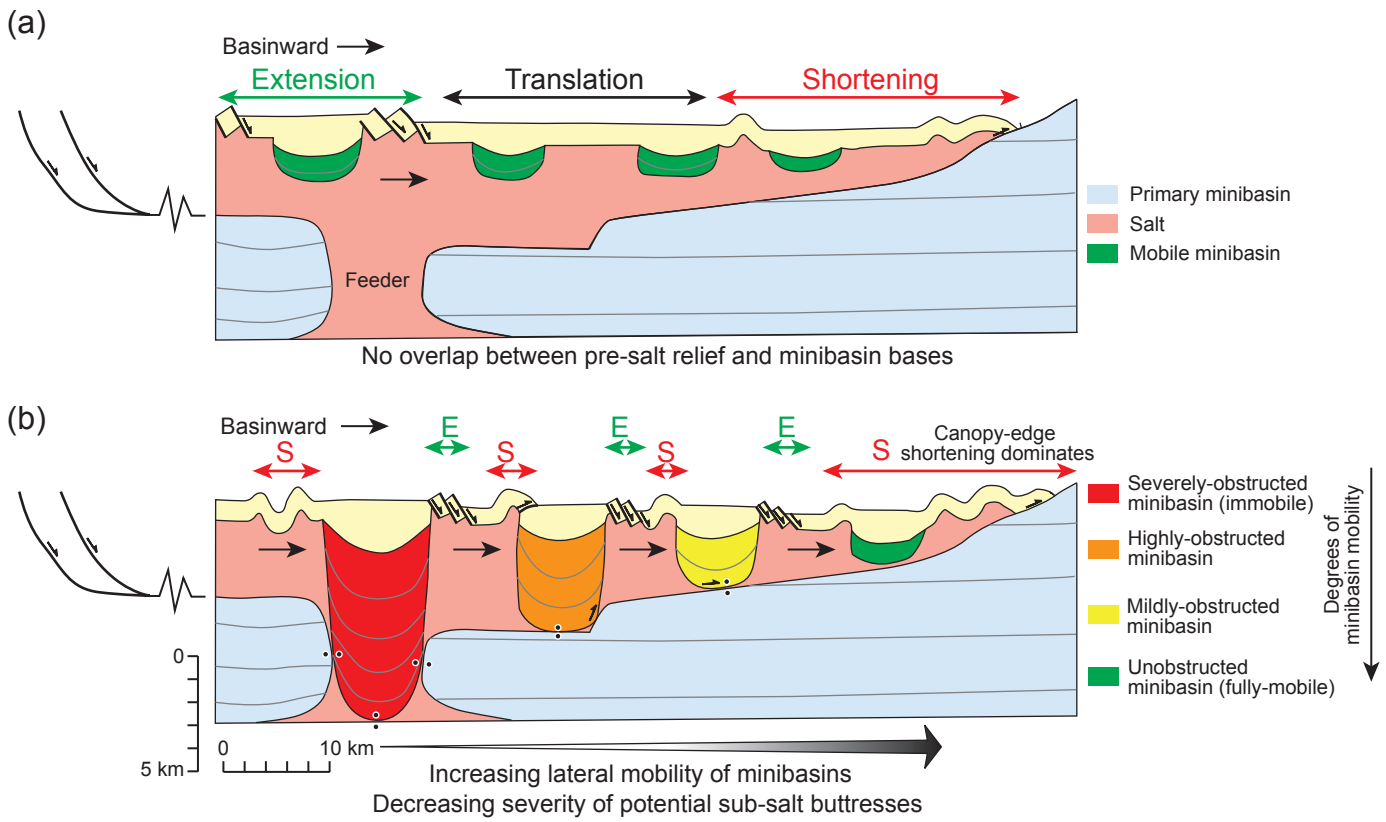
(a)
Basinward
Extension
Translation
Shortening
Feeder
Primary minibasin
Salt
Mobile minibasin
No overlap between pre-salt relief and minibasin bases
(b)
Basinward
E
S
Canopy-edge
shortening dominates
Severely-obstructed
minibasin (immobile)
Highly-obstructed
minibasin
Mildly-obstructed
minibasin
Unobstructed
minibasin (fully-mobile)
Degrees of
minibasin mobility
0
5 km
0
10 km
Increasing lateral mobility of minibasins
Decreasing severity of potential sub-salt buttresses

Figure 15

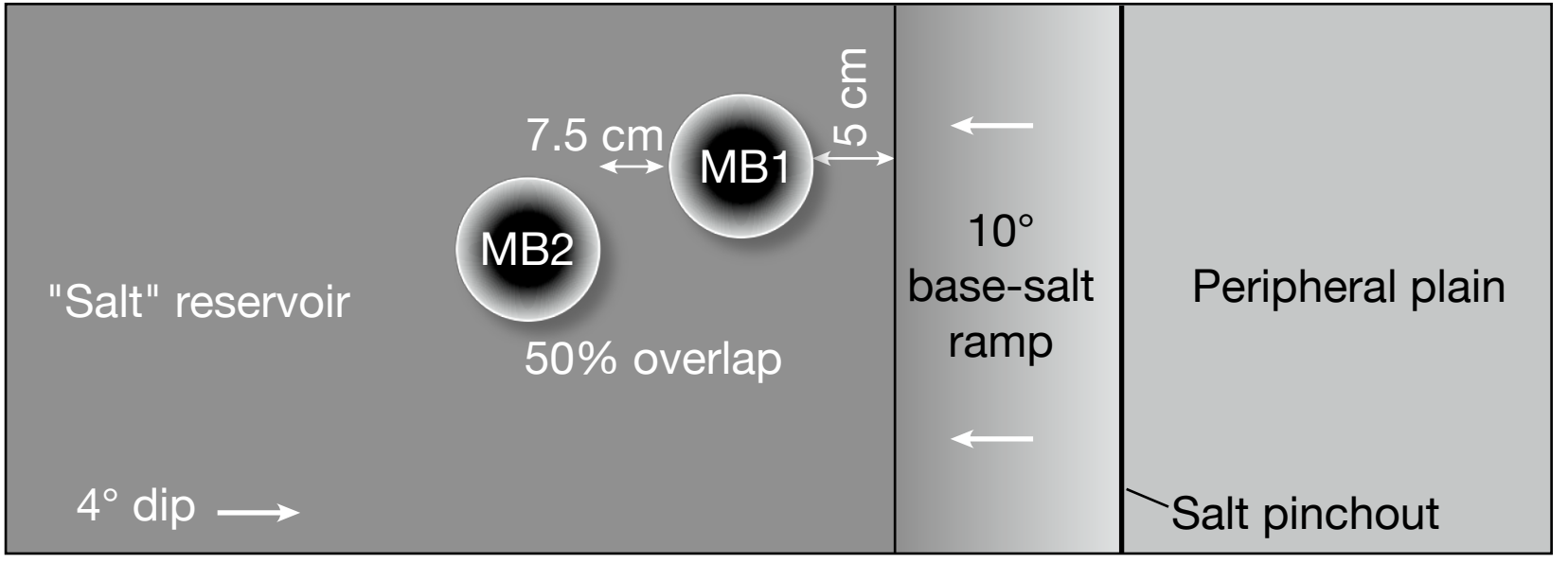
7.5 cm
5 cm
MB1
MB2
"Salt" reservoir
50% overlap
10°
base-salt
ramp
Peripheral plain
4° dip
Salt pinchout

Figure A1